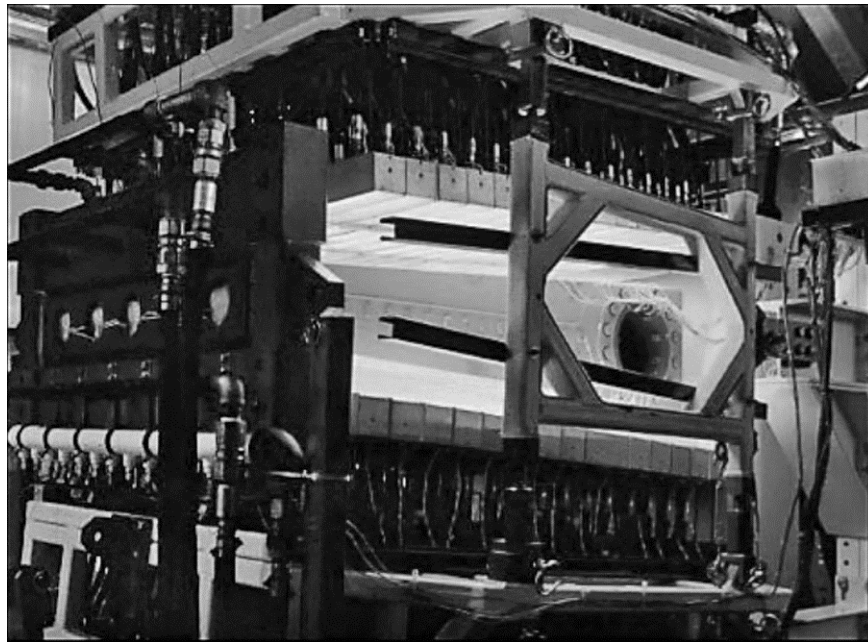# Proportional and Integral Thermal Control System for Large Scale Heating Tests

*Van Tran Fleischer*
*Armstrong Flight Research Center, Edwards, Califomia*

# NASA STI Program ... in Profile

Since its founding, NASA has been dedicated to the advancement of aeronautics and space science. The NASA scientific and technical information (STI) program plays a key part in helping NASA maintain this important role.

The NASA STI program operates under the auspices of the Agency Chief Information Officer. It collects, organizes, provides for archiving, and disseminates NASA's STI. The NASA STI program provides access to the NASA Aeronautics and Space Database and its public interface, the NASA Technical Reports Server, thus providing one of the largest collections of aeronautical and space science STI in the world. Results are published in both non-NASA channels and by NASA in the NASA STI Report Series, which includes the following report types:

- TECHNICAL PUBLICATION. Reports of completed research or a major significant phase of research that present the results of NASA Programs and include extensive data or theoretical analysis. Includes compila-tions of significant scientific and technical data and information deemed to be of continuing reference value. NASA counter-part of peer-reviewed formal professional papers but has less stringent limitations on manuscript length and extent of graphic presentations.

- TECHNICAL MEMORANDUM. Scientific and technical findings that are preliminary or of specialized interest, e.g., quick release reports, working papers, and bibliographies that contain minimal annotation. Does not contain extensive analysis.

- CONTRACTOR REPORT. Scientific and technical findings by NASA-sponsored contractors and grantees.

- CONFERENCE PUBLICATION. Collected papers from scientific and technical conferences, symposia, seminars, or other meetings sponsored or co-sponsored by NASA.

- SPECIAL PUBLICATION. Scientific, technical, or historical information from NASA programs, projects, and missions, often concerned with subjects having substantial public interest.

- TECHNICAL TRANSLATION. English-language translations of foreign scientific and technical material pertinent to NASA's mission.

Specialized services also include organizing and publishing research results, distributing specialized research announcements and feeds, providing information desk and personal search support, and enabling data exchange services.

For more information about the NASA STI program, see the following:

- Access the NASA STI program home page at http://www.sti.nasa.gov

- E-mail your question to help@sti.nasa.gov

- Phone the NASA STI Information Desk at 757-864-9658

- Write to:
  NASA STI Program
  Mail Stop 148
  NASA Langley Research Center
  Hampton, VA 23681-2199

NASA/TM—2015–218721
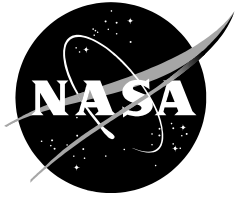
# Proportional and Integral Thermal Control System for Large Scale Heating Tests

*Van Tran Fleischer*
*Armstrong Flight Research Center, Edwards, Califomia*

**June 2015**

# Table of Contents

# ABSTRACT

The National Aeronautics and Space Administration Armstrong Flight Research Center (Edwards, California) Flight Loads Laboratory is a unique national laboratory that supports thermal, mechanical, thermal/mechanical, and structural dynamics research and testing. A Proportional Integral thermal control system was designed and implemented to support thermal tests. A thermal control algorithm supporting a quartz lamp heater was developed based on the Proportional Integral control concept and a linearized heating process. The thermal control equations were derived and expressed in terms of power levels, integral gain, proportional gain, and differences between thermal setpoints and skin temperatures. Besides the derived equations, user's predefined thermal test information generated in the form of thermal maps was used to implement the thermal control system capabilities. Graphite heater closed-loop thermal control and graphite heater open-loop power level were added later to fulfill the demand for higher temperature tests. Verification and validation tests were performed to ensure that the thermal control system requirements were achieved. This thermal control system has successfully supported many milestone thermal and thermal/mechanical tests for almost a decade with temperatures ranging from 50 °F to 3000 °F and temperature rise rates from -10 °F/s to 70 °F/s for a variety of test articles having unique thermal profiles and test setups.

# NOMENCLATURE

| | |
|---|---|
| A/D | analog-to-digital converter |
| ACP | acquisition and control processor |
| *acoeff* | A coefficient |
| ANSI | American National Standards Institute |
| AFRC | Armstrong Flight Research Center |
| *bcoeff* | B coefficient |
| *c, C* | controlled variable, skin temperature, ºF |
| C/C | carbon/carbon |
| CLM | closed-loop map |
| CMC | ceramic matrix composite |
| C/SiC | carbon silicon carbide |
| *d* | number of delay cycles |
| DACS | Data Acquisition and Control System |
| D/A | digital-to-analog converter |
| *e, E* | thermal setpoint minus skin temperature |
| *F* | number of cycles per second |
| FLL | Flight Loads Laboratory |
| GH | graphite heater |
| I | current signal |
| Im (z) | imaginary axis in the *z*-domain |
| $K_i$ | integral gain coefficient |
| $K_p$ | proportional gain coefficient |
| *n-1, n, n+1* | discrete time |
| NASA | National Aeronautics and Space Administration |
| PCC | power control cabinet |
| PCM | profile control map |
| PI | Proportional and Integral |
| QL | quartz lamp |
| QL_GH | quartz lamp and graphite heater |
| SpecId | specimen identification |
| Re (z) | real axis in the *z*-domain |

| SCR | silicon controlled rectifiers |
|---|---|
| $t$ | time |
| TC | thermocouple |
| TCS | thermal control system |
| THRM PET | thermal profile elapsed time |
| $r, R$ | reference input, thermal setpoint, ºF |
| $u, U$ | controller output, power level |
| $z$ | z-transform variable |
| $\alpha$ | integral sensitivity factor |
| $\beta$ | proportional sensitivity factor |
| $\Delta t$ | time interval, second |

# INTRODUCTION

A Proportional Integral (PI) closed-loop thermal control system (TCS) was built in-house to support large-scale heating tests at the National Aeronautics and Space Administration (NASA) Armstrong Flight Research Center (AFRC) Flight Loads Laboratory (FLL) in Edwards, California. A complete TCS includes mathematical models, algorithm, hardware, and software. This report emphasizes the mathematical models and algorithm; it does not describe the TCS supporting hardware and software. The TCS consists of two basic parts: controller and heating process. The controller includes a real-time operating system acquisition and control processor (ACP), input modules or analog-to-digital (A/D) converters, and output modules or digital-to-analog (D/A) converters. The heating process contains a power control cabinet (PCC), quartz lamp (QL) heaters, and control thermocouples (TC)s.

The design of the TCS involved a popular PI control model and a linearized heating process model (ref. 1). The equations that represent the models were mathematically derived at first in continuous-time domain, and later changed to discrete-time domain or *z*-domain (ref. 2) to be implemented in a real-time operating computer system. Then, the two models were combined to derive the closed-loop TCS transfer function and stability region. With some reasonable assumptions to simplify the mathematical derivation process, a closed-loop TCS transfer function in the *z*-domain was achieved, and a stability region was determined. A method to calculate the integral gain $K_i$ and the proportional gain $K_p$ was developed so that the gains were within the stability region. The derived thermal control equations and thermal maps that contain important information were used to implement and to add new capabilities. The thermal control algorithm was written in American National Standards Institute (ANSI) C programming language to build the TCS that met all of the QL thermal control system requirements (ref. 3). The executable code of the thermal control algorithm was loaded into the ACP (ref. 4), a component of the FLL Data Acquisition and Control System (DACS). Since the PCC is the main component of the heating process, the operation of the PCC zero crossover is described to explain the role of the PCC in the derivation of the thermal control equations and its function of firing the QL to provide radiant heat.

In 2005, graphite heater (GH) power control cabinets were integrated into the TCS to support heating tests with temperatures up to 3000 ºF. In 2006, GH closed-loop thermal control capability was added in the TCS using the derived thermal control equations and software control logic based on test data and the GH high thermal inertia characteristics. The GH closed-loop thermal control software was tested in a small test chamber that can support up to 2 zones. When finished, the GH closed-loop thermal control had all the capabilities applied to the QL closed-loop thermal control.

In 2008, GH open-loop power level capability was added to allow the TCS to fire the GH with predefined power levels programmed in the thermal maps. Since GH has high thermal inertia, control TC was required

in each zone to monitor the highest temperature limit for safety. The GH open-loop power level was also achieved using the small test chamber.

In 2010, both QL and QH were installed in a test setup for very high temperature tests. The TCS produced high power levels to provide heating conditions with temperatures up to 3000 ºF and with high temperature rise rates.

From 2003 to 2010, this TCS had performed many large-scale heating tests with either QL, or GH, or both QL and GH (QL_GH). The TCS had successfully accomplished the criteria of all thermal-structural test programs operating in the FLL. With this robust and diversified TCS, the FLL was able to support hot structural research for advanced aerospace programs including milestone thermal and thermal/mechanical tests that had never been done before.

# QUARTZ LAMP THERMAL CONTROL SYSTEM DESIGN

The design of the QL TCS involves a controller and a heating process as shown in figure 1. The controller outputs the required power level to the heating process to heat a test specimen following a preplanned thermal profile. The algorithm of the closed-loop TCS starts in continuous-time and then converts to discrete-time. Since computers run their tasks repeatedly every cycle, the discrete-time model must be developed using the z-domain.

## PI Control System Model

The PI controller was selected in the design of the TCS. This algorithm involves two separate parameters: the proportional $P$ depends on the present error, and the integral $I$ depends on the accumulation of past errors. The PI controller block diagram is described in figure 2 with the assumption that at the initial time $t_0$, controller output $u(t_0) = 0$. Equation (1) is the mathematical representation of the PI controller;

$$u(t) = K_i \int_{t_0}^{t} e(\tau)\, d\tau + K_p e(t) \tag{1}$$

in which $t$ is the current time, $t_0$ is the initial time, $\tau$ is the variable of integration taking on values from time 0 to the current time $t$, $r$ is the reference input, $c$ is the controlled variable, $e = r - c$ is the difference between $r$ and $c$, $u(t)$ is the controller output at time $t$, $K_i$ is the integral gain, and $K_p$ is the proportional gain. By taking derivative of equation (1), the control model can be described by the differential equation (2):

$$\frac{du}{dt} = K_i e + K_p \frac{de}{dt} \tag{2}$$

Integrating equation (2) from time $t_{n-1}$ to time $t_n$ with the time interval $\Delta t = t_n - t_{n-1}$ is shown in equation (3):

$$\int_{t_{n-1}}^{t_n} du = K_i \int_{t_{n-1}}^{t_n} e d\tau + K_p \int_{t_{n-1}}^{t_n} de \tag{3}$$

Equation (3) can be integrated to yield equation (4):

$$U_n = U_{n-1} + K_i \int_{t_{n-1}}^{t_n} e d\tau + K_p(E_n - E_{n-1}) \tag{4}$$

where $U_n$ is the controller output at time $n$, $U_{n-1}$ is the controller output at time $n$-1, $E_n = R_n - C_n$ is the difference between reference input and controlled variable at time $n$, $E_{n-1} = R_{n-1} - C_n - 1$ is the difference between reference input and controlled variable at time $n$-1, $\tau$ is the variable of integration taking on values from time $t_{n-1}$ to time $t_n$. $\int_{t_{n-1}}^{t_n} e d\tau$ is calculated by linear approximation, and roughly equals the area of the surface shown in figure 3, the area of a trapezoid with the bases $E_n$ and $E_{n-1}$, and the height of $\Delta t$. The integral part of equation (4) can be expressed in equation (5):

$$\int_{t_{n-1}}^{t_n} e d\tau \cong \Delta t \frac{E_n + E_{n-1}}{2} \tag{5}$$

The following equation is obtained by combining equations (4) and (5). The equivalent discrete-time model is expressed below in equation (6):

$$U_n = U_{n-1} + K_i \frac{\Delta t}{2}(E_n + E_{n-1}) + K_p(E_n - E_{n-1}) \tag{6}$$

Expand equation (6) and rearrange the terms (see Appendix A), the equation of the discrete-time PI control model is derived as equation (7):

$$U_n = U_0 + K_i \Delta t \left[ \sum_{j=0}^{n} E_j - \left( \frac{E_n + E_0}{2} \right) \right] + K_p(E_n - E_0) \tag{7}$$

There is always an inherit delay in any control system. Equation (7) allows $U_n$ to be calculated from $U_0$; therefore, $U_n$ can also be calculated from $U_{n-d}$, where $d$ is the number of delay cycles between the commanded controller output $U_{n-d}$ to get the reference input $R_{n-d}$ at time $n$-$d$ and its current corresponding controlled variable $C_n$ at time $n$. Replacing time $n - d$ for time 0 in equation (7) gives equation (8):

$$U_n = U_{n-d} + K_i \Delta t \left[ \sum_{j=n-d}^{n} E_j - \left( \frac{E_n + E_{n-d}}{2} \right) \right] + K_p(E_n - E_{n-d}) \tag{8}$$

Equation (8) is much more practical than equation (7) since the computer can easily store $d$ values of $U$ and $E$ before the current cycle or time $n$, but not from starting time 0. Let time interval $\Delta t = 1$ s and $F$ be the number of cycles per second, then the controller output $U_n$ at time $n$ is determined as follows in equation (9):

$$U_n = \frac{1}{F}\left\{U_{n-d} + K_i\left[\sum_{j=n-d}^{n} E_j - \left(\frac{E_n + E_{n-d}}{2}\right)\right] + K_p(E_n - E_{n-d})\right\} \tag{9}$$

Equation (9) is the controller output equation derived from the PI control model. Equation (9) is the general closed-loop PI control equation and can be used for any PI control system with controller output $U$. For the thermal control system, $R$ is the thermal setpoint, $C$ is the skin temperature, $E = R - C$ is the difference between thermal setpoint and skin temperature, and $U$ is the power level.

## Heating Process Model

A nonlinear continuous-time model for the heating process is described generally as follows in equation (10):

$$\frac{dc}{dt} = \frac{K_1}{K_2}(u^4 - c^4) = f(c, u) \tag{10}$$

where $c$ is the skin temperature, $u$ is the power level, and $f(c,u)$ is a function of $c$ and $u$. To the above nonlinear system, a simplified linear model of the heating process model described in figure 4 is used and expressed mathematically in equation (11):

$$\frac{dc}{dt} = ac + bu + g \tag{11}$$

Where $a, b, g$ coefficients are not constants and are functions of outside temperatures. The equivalent discrete heating process model is obtained at times $n$ and $n+1$ with the time interval $\Delta t = t_{n+1} - t_n$ as shown in equation (12):

$$\frac{C_{n+1} - C_n}{\Delta t} = aC_n + bU_n + g \tag{12}$$

Move the term $C_{n+1}$ in equation (12) to the left side as in equation (13):

$$C_{n+1} = (1 + a\Delta t)C_n + b\Delta t U_n + g\Delta t \tag{13}$$

To have equation (13) expressed in a more compact form, the coefficients of equation (13) are defined in equations (14), (15), and (16):

$$A = 1 + a\Delta t \tag{14}$$

$$B = b\Delta t \tag{15}$$

$$G = g\Delta t \tag{16}$$

Equation (13) can be written as equation (17):

$$C_{n+1} = AC_n + BU_n + G \tag{17}$$

Based upon the inherit delay in any control system, it is assumed that the power level $U$ applied at the beginning, $n = 0$, does not cause any changes in the specimen skin temperature.

At $n = 0$, $U_0 = 0$, and $C_{n+1} = C_n = C_0$, equation (17) can be expressed as equation (18):

$$C_0 = AC_0 + G \tag{18}$$

Moving all the $C_0$ terms to one side yields equation (19):

$$G = C_0 - AC_0 \tag{19}$$

Equation (19) defines a coefficient $G$ based on initial temperature $C_0$ and coefficient $A$. Substituting $G$ into equation (17) gives equation (20):

$$C_{n+1} = AC_n + BU_n + C_0 - AC_0 \tag{20}$$

Grouping the $A$ terms yields equation (21):

$$C_{n+1} = A(C_n - C_0) + BU_n + C_0 \tag{21}$$

Equation (21) is the heating process equation.

### Closed-Loop Thermal Control Transfer Function

After deriving the PI control equation (9) and the heating process equation (21), the PI control model and the heating process model are combined as shown in figure 5 so that the closed-loop thermal control transfer function can be developed. The transfer function provides a basis for determining important control-system response characteristics and stability.

The time interval in the control and the time interval in the heating process are assumed to be equal. Rearrange terms in equation (21) (see Appendix B); the relationship between the controlled variable and the reference input can be written as follows in equation (22):

$$C_{n+1} = C_n \left( A - BK_p + BK_i \frac{\Delta t}{2} \right) + R_n \left( BK_p - BK_i \frac{\Delta t}{2} \right) + BK_i \Delta t \left( \sum_{j=0}^{n} R_j - \sum_{j=0}^{n} C_j \right) + I_0 \tag{22}$$

where $A$ and $B$ represent the coefficients of the test specimen and are functions of temperatures, and

$$I_0 = C_0 - AC_0 - BK_i \frac{\Delta t}{2} R_0 + BK_i \frac{\Delta t}{2} C_0 - BK_p R_0 + BK_p C_0 \tag{23}$$

Equation (23) represents a constant at the initial time $n = 0$ and is defined based on the initial conditions of $A, B, K_i$, and $K_p$.

In order to derive the transfer function of the TCS, equation (22) must be transformed to the $z$-domain (see Appendix C). The equivalent $z$-transform of equation (22) is described as follows in equation (24):

$$
\begin{aligned}
C(z) &\left[ 1 - z^{-1}\left( 1 + A - BK_p - BK_i \frac{\Delta t}{2} \right) + z^{-2}\left( A - BK_p + BK_i \frac{\Delta t}{2} \right) \right] \\
&= R(z)\left[ z^{-1}\left( BK_p + BK_i \frac{\Delta t}{2} \right) - z^{-2}\left( BK_p - BK_i \frac{\Delta t}{2} \right) \right] + z^{-1}(I_0 - C_0) \\
&+ C_0
\end{aligned}
\tag{24}
$$

where $I_0 - C_0$ and $C_0$ are initial condition terms at time $n = 0$. To simplify the developing process, these terms are assumed negligible and ignored. Equation (24) can be written as equation (25):

$$\frac{C(z)}{R(z)} = \frac{z^{-1}\left( BK_p + BK_i \frac{\Delta t}{2} \right) - z^{-2}\left( BK_p - BK_i \frac{\Delta t}{2} \right)}{1 - z^{-1}\left( 1 + A - BK_p - BK_i \frac{\Delta t}{2} \right) + z^{-2}\left( A - BK_p + BK_i \frac{\Delta t}{2} \right)} \tag{25}$$

To simplify equation (25), two new values $\alpha$ and $\beta$ are introduced as follows in equations (26) and (27):

$$\alpha = \frac{K_i}{K_p} \Delta t \tag{26}$$

$$\beta = BK_p \tag{27}$$

where $\alpha$ is called the integral sensitivity factor, and $\beta$ is called the proportional sensitivity factor. Both values of $\alpha$ and $\beta$ must be positive numbers, $\alpha > 0.0$ and $\beta > 0.0$. Considering equation (14), $A = 1 + a\Delta t$ is dependent on coefficient $\alpha$, a function of outside temperature.

The effect of outside temperature is assumed minimal, $a = 0$ and equation (14) becomes $A = 1$. Replacing $\alpha$ and $\beta$ into equation (25), a simpler form as in equation (28) is achieved:

$$\frac{C(z)}{R(z)} = \frac{z^{-1}\left( \beta + \frac{\alpha\beta}{2} \right) - z^{-2}\left( \beta - \frac{\alpha\beta}{2} \right)}{1 - z^{-1}\left( 2 - \beta - \frac{\alpha\beta}{2} \right) + z^{-2}\left( 1 - \beta + \frac{\alpha\beta}{2} \right)} \tag{28}$$

7

Multiplying both the denominator and numerator with $z^2$, the transfer function can be written in the form of the powers of z as shown in equation (29):

$$\frac{C(z)}{R(z)} = \frac{\left(\beta + \frac{\alpha\beta}{2}\right)z - \left(\beta - \frac{\alpha\beta}{2}\right)}{z^2 - \left(2 - \beta - \frac{\alpha\beta}{2}\right)z + \left(1 - \beta + \frac{\alpha\beta}{2}\right)} \tag{29}$$

Equation (29) is the closed-loop thermal control transfer function.

## Thermal Control System Stability

In the *z*-domain, the control system is stable if the poles of equation (29) lie inside the unit circle in the *z*-plane. Normally, the poles of a control system have two parts: the real part and the imaginary part. This thermal control system is designed by assigning specific values to the poles that are on the real axis and on the right-hand side inside the unit circle. These poles have the real part and no imaginary part. This assignment leads to $0 < z_1, z_2 < 1$ as shown in figure 6, and equations (30) and (31):

$$0 < z_1, z_2 = \frac{\left(2 - \beta - \frac{\alpha\beta}{2}\right) \pm \sqrt{\left(2 - \beta - \frac{\alpha\beta}{2}\right)^2 - 4\left(1 - \beta + \frac{\alpha\beta}{2}\right)}}{2} < 1 \tag{30}$$

$$\left(2 - \beta - \frac{\alpha\beta}{2}\right)^2 - 4\left(1 - \beta + \frac{\alpha\beta}{2}\right) \geq 0 \tag{31}$$

Solving equations (30) and (31) (see Appendix D), a TCS stability region is determined as shown in figure 7. The selection of the values of α and β in the stability region must be done carefully since these values are used in the calculation of $K_i$ and $K_p$. If the proportional gain is too high, the system can become unstable. In contrast, if the proportional gain is too small the system can become less robust or less sensitive. The proportional term of a PI control system contributes the bulk of the output change. The integral term responds to accumulated errors from the past and can cause overshooting the setpoint. After tuning the control parameters, the values of α = 0.35 and β = 1.1 were selected inside the system stability region.

## Integral Gain $K_i$ and Proportional Gain $K_p$

In order to determine $K_i$ and $K_p$ gains that are included in the closed-loop PI control equation (9), a pre-test open-loop specimen identification (SpecId) test is run. The purpose of this test is to compute A and B coefficients denoted as *acoeff* and *bcoeff*, which will be discussed later in this section. The A and B coefficients along with α and β factors are used in the calculations of $K_i$ and $K_p$ gains.

For each SpecId test, a maximum SpecId temperature, a minimum SpecId temperature, and each zone low power level per cycle (not per second) must be preplanned. The maximum SpecId temperature should not be too high since it may damage a test specimen in an open test environment, and the minimum SpecId temperature should not be too low since it will take a long time to finish the test. There are two phases in a SpecId test: a heating phase with low power level and a cooling phase with no power. When any control TC

reaches the maximum SpecId temperature; the heating phase is finished, power is turned off, and natural cooling occurs. When all control TCs reach the minimum SpecId temperature, the SpecId test is complete. New *acoeff* and *bcoeff* coefficients are defined as follows in equations (32) and (33):

$$acoeff = -a \tag{32}$$

$$bcoeff = \frac{1}{b} \tag{33}$$

Coefficient *acoeff* is calculated during the cooling phase. Consider equation (11):

$$\frac{dc}{dt} = ac + bu + g \tag{11}$$

At $t = 0$, $u = 0$, $\frac{dc}{dt} = 0$, and $c = c_0$ where $c_0$ is the initial ambient temperature and $g = -ac_0$. Substitution of $g = -ac_0$ into equation (11) yields equation (34):

$$\frac{dc}{dt} = a(c - c_0) + bu \tag{34}$$

During the cooling phase there is no power; so $u = 0$ and as shown in equation (35):

$$\frac{dc}{dt} = a(c - c_0) = -a(c_0 - c) \tag{35}$$

Replacing equation (32) into equation (35) can be expressed as equation (36):

$$acoeff = \frac{dc}{dt}\left(\frac{1}{c_0 - c}\right) \tag{36}$$

During the heating phase, $u$ is a low constant power level. Using equations (32) and (33), $u$ can be expressed in *acoeff* and *bcoeff* coefficients as equations (37) and (38):

$$u = \frac{1}{b}\left[\frac{dc}{dt} - a(c - c_0)\right] = bcoeff\left[\frac{dc}{dt} + acoeff(c - c_0)\right] \tag{37}$$

$$bcoeff = \frac{u}{\frac{dc}{dt} + acoeff(c - c_0)} \tag{38}$$

Equations (36) and (38) are used during SpecId to calculate *acoeff* and *bcoeff* coefficients. For a real-time computer system, the calculation of power levels is carried out in each time *n,* and as mentioned earlier, *F* is the number of cycles per second. The power level at time *n* can be expressed as follows in equation (39):

9

$$U_n = \frac{1}{F}\left\{bcoeff\left[\frac{dc}{dt} + acoeff(c - c_0)\right]\right\} \tag{39}$$

Equation (39) is the controller output equation derived from the heating process model and is only used for the first five seconds at the beginning of a thermal test for any QL heater zones.

Figure 8 shows in detail how *acoeff* and *bcoeff* are calculated. During the cooling phase, $c_{H2}$ is the starting temperature at the start time $t_{H2}$, and $c_{L2}$ is the ending temperature at the end time $t_{L2}$ of the selected temperature range, $c_c$ is the midpoint temperature of $c_{H2}$ and $c_{L2}$ as shown in equation (40):

$$c_c = \frac{c_{H2} + c_{L2}}{2} \tag{40}$$

and the slope of skin temperature versus time is expressed in equation (41):

$$\frac{dc}{dt} = \frac{c_{H2} - c_{L2}}{t_{H2} - t_{L2}} \tag{41}$$

Because of the delay, the temperature continues to rise for a short time after the heating phase is done, and the power is turned off. The first selected cooling temperature range should be chosen well below the temperature peak to ensure the equivalent heating temperature range is in the heating phase with $u > 0.0$. The initial ambient temperature $c_0$ is always less than the midpoint temperature $c_c$, where $c_0 - c_c < 0.0$, and the temperature is always decreasing with time for the cooling phase, $dc/dt < 0.0$; therefore, *acoeff* is always positive. Equation (36) is used to calculate *acoeff*.

For the equivalent heating phase, the midpoint temperature $c_h$ must be selected as closely as possible to the cooling phase midpoint temperature $c_c$ within ±1.0 °F. Let $c_{L1} = c_h - \Delta c$ be the starting temperature at the start time $t_{L1}$, and $c_{H1} = c_h + \Delta c$ is the ending temperature at the end time $t_{H1}$ of the selected temperature range, and the slope of skin temperature versus time is shown in equation (42):

$$\frac{dc}{dt} = \frac{c_{H1} - c_{L1}}{t_{H1} - t_{L1}} \tag{42}$$

The initial ambient temperature $c_0$ is always less than the midpoint temperature $c_h$, $c_h - c_0 > 0.0$, and the temperature is always increased with time during the heating phase, $dc/dt > 0.0$; therefore, *bcoeff* is always positive. Equation (38) is used to calculate *bcoeff*.

The above calculation is for one control TC and for one selected temperature range. Many more selected temperature ranges should be used to calculate *acoeff* and *bcoeff*. The final *acoeff* and *bcoeff* values are the average of all the calculated values.

The integral gain $K_i$ and the proportional gain $K_p$ can be determined from equations (15), (26), and (27). With the time interval $\Delta t = 1$ s, equation (15) becomes: $B = b$, and equation (27) becomes equation (43):

$$K_p = \frac{\beta}{B} = \frac{\beta}{b} \tag{43}$$

By replacing $1/B = 1/b = bcoeff$ into the above equation, $K_p$ can be expressed as equation (44):

$$K_p = \beta bcoeff \tag{44}$$

Equation (44) is the equation used in the calculation of $K_p$.
With the time interval $\Delta t$ equal to one second, equation (26) can be written as equation (45):

$$K_i = \alpha K_p \tag{45}$$

Equation (45) is the equation used in the calculation of $K_i$.

### Power Control Cabinet

In order to implement the TCS, an understanding of the operation of the PCC is necessary. The PCC is actually the main component of the heating process mentioned in the QL TCS design. For each control TC at time $n$, the ACP uses the delayed power level $U_{n-d}$, the skin temperatures $C_{n-d}$ and $C_n$, the thermal setpoints $R_{n-d}$ and $R_n$, $K_i$, and $K_p$ to calculate power level $U_n$ which is a real number ranging from 0 to 60/$F$ power levels. Since the ACP calculates the power level 5 times per second ($F = 5$), $U_n$ value ranges from 0.0 to 12.0 power levels per cycle. The ACP translates $U_n$ into a format suitable for interfacing with the output module or D/A converter. After receiving the signal from the ACP, the output module converts it into the current signal $I$ between 4.0 mA and 20.0 mA and sends it to the PCC which fires the QL heater installed above the control. TC attached on a test article or an individual test coupon. Then, the temperature feedback from the control TC is input into the ACP for closed-loop control.

The PCC is a back-to-back silicon controlled rectifier (SCR) zero crossing controller that operates on 60 Hz or 60 power levels per second (ref. 5). For the circuit configuration in figure 9, the SCRs must be connected in parallel, but opposite directions. The forward SCR conducts during the positive half of the cycle, and the reverse SCR conducts during the negative half of the cycle to allow both halves of the AC waveform. In AC, the zero-crossing is the instantaneous point with no voltage or current where the sine wave goes from negative to positive or from positive to negative. The zero crossing detector senses the zero crossing of the AC voltage/current input, and the SCR is turned on. The benefits of zero crossing are very low harmonics and radio frequency interference. The PCC has zero crossover firing mode that distributes even on/off cycles to provide the desired percentage output based on the current signals in mA sending to the SCRs. The QL heater is fired when the zero-crossing occurs where the sine wave goes from negative to positive as shown in figure 10a. Table 1 and figures 10a to 10c demonstrate the relationships between the current signals $I$ to the SCRs, percentages of full power, number of cycles on/off, power level per second, and power level per cycle.

Table 1. Relationships between current signals *I* to SCRs, percentage of full power, number of cycles on/off, and power levels.

| Signals to SCRs, mA | Percentage of full power | Number of cycles on/off | Power levels per second | Power levels per cycle |
|---|---|---|---|---|
| 20.0 | Full on | all cycles on | 60 | 60/*F* |
| 16.0 | 75% | 3 cycles on, 1 cycle off | 45 | 45/*F* |
| 12.0 | 50% | 1 cycle on, 1 cycle off | 30 | 30/*F* |
| 8.0 | 25% | 1 cycle on, 3 cycles off | 15 | 15/*F* |
| 4.0 | Full off | All cycles off | 0 | 0 |

## QUARTZ LAMP THERMAL CONTROL SYSTEM IMPLEMENTATION

Equations (9) and (39) by themselves cannot build the TCS; other important information is required to build the TCS. The required information such as test type, heater type, zone type, and thermal profiles was preplanned, created, compiled, and loaded in binary format in the ACP before any thermal test and is called a thermal map. A thermal map contains a series of important information that instructs the TCS to perform its intended tasks. The implementation of the QL thermal control algorithm written in ANSI C was based on the derived thermal control equations and thermal maps.

To implement thermal control, besides coding, a small four-zone setup was built with 4 input modules, 4 Type-K control TCs, 4 individual test coupons, 4 output modules, and 4 infrared heated lamps. The test setup was covered with an insulation blanket to minimize the effect of natural and forced convection. The test setup was limited to a maximum temperature of 350 ºF for safety. When the TCS algorithm proved to be working with the small setup, a larger setup similar to the one shown in figure 11 with 18 QL zones and 18 different test coupons separated by insulated ceramic walls. Each zone has a QL heater installed on the lid and a Type-K control TC attached on top of a test coupon. Figure 12 shows a typical control TC attached on top of a test coupon. Figure 13 shows a typical single quartz lamp bulb. Figure 14 shows a QL carbon/carbon (C/C) elevon large-scale heating test in the FLL using the PI TCS.

# Thermal Control Equations

The key of the thermal control system is the derived thermal control equations (9) and (39) from which the ACP calculates power level every 200 ms. Equation (9) is the closed-loop control equation and the main equation to calculate power level.

## *Equation derived from the PI controller*

Power level at time *n* is calculated using the closed-loop thermal control equation (9):

$$U_n = \frac{1}{F}\left\{ U_{n-d} + K_i \left[ \sum_{j=n-d}^{n} E_j - \left( \frac{E_n + E_{n-d}}{2} \right) \right] + K_p(E_n - E_{n-d}) \right\} \tag{9}$$

The calculated power level ranging from 0.0 to 12.0 per cycle must be converted to a suitable integer number to the assigned output module (D/A). Upon receiving the input signal, the output module sends the corresponding current signal to the assigned PCC channel which will fire its connected QL heater. The zone control TC sends the feedback temperature to the ACP via the assigned input module (A/D). The ACP uses the feedback temperatures along with the profile setpoints and the power level at time *n-d* to calculate the power level at the current time *n*.

## *Equation derived from the heating process*

Power level at time *n* is calculated using equation (39):

$$U_n = \frac{1}{F}\left\{ bcoeff \left[ \frac{dc}{dt} + acoeff(c - c_0) \right] \right\} \tag{39}$$

At the beginning of a thermal test, equation (39) is only used for 5 s to calculate power level at time *n*. When enough data is saved, equation (39) is no longer used.

# Thermal Maps

Three thermal maps: a profile control map (PCM), a closed-loop map (CLM), and a power output map were created to implement the TCS. Each map contains important information that is used in the thermal control algorithm and is described in the following sections.

## *Profile Control Map*

The PCM consists of preplanned thermal profiles in segment format for all control TCs. Each segment contains start time, end time, start temperature, end temperature, and other important information. The ACP uses the data programmed in each segment to calculate thermal setpoints and to make decisions in executing its tasks. The programmed capabilities such as limit checking, average power level, maximum power level, and feedback temperature sensor switching are preplanned in each segment. The graph in figure 15 displays a thermal profile defined in Appendix E that has 8 segments with the highest temperature at 1480 ºF and the thermal profile time of 1200 s.

The PCM has the number of control TCs, test type (SpecId, replay power level, closed-loop, or open-loop power level), heater type (QL, or GH, or QL_GH), PCC used in the test, number of control delay cycles, SpecId maximum temperature, SpecId minimum temperature, maximum ramp up rate, and more.

*Closed-Loop Map*

The CLM holds the information that links which PCC channel and which control TC belong to which zone, which zone is master, and which zone is slave. A master zone always has its assigned control TC, and power level is calculated for this zone using the thermal control equation (9). A master zone can have none, one, or multiple slave zones. A slave zone does not have any control TC and is assigned to a master zone. A slave zone is fired with the same power level as its master zone. The CLM also has each zone heater type (QL or GH), SpecId power level, temperature limits including highest, lowest, high deviation, and low deviation. A deviation equals to a thermal setpoint at time *n-d* $R_{n-d}$ minus its corresponding skin temperature at current time $C_n$ (deviation = $R_{n-d} - C_n$). The TCS is underheated when the deviation is positive and overheated when the deviation is negative. There are three zone configurations: one PCC channel for one control TC (most common), one PCC channel for multiple control TCs (feedback temperature sensor switching), and one PCC channel with no control TC (slave zone). Since a zone can have one or multiple control TCs, and also since the slave zone doesn't have a control TC, the number of PCC channels and the number of control TCs may not be the same.

*Power Output Map*

The PCM contains the number of zones and the physical addresses of all output modules used in the test. The zone defined in the CLM is linked to this map.

# THERMAL CONTROL SYSTEM CAPABILITIES

The TCS capabilities are categorized into three different types: interactive, programmed, and pre-test. The interactive type must be triggered by an operator's action. The programmed type must be preplanned and programmed in the thermal maps. The pre-test type must be done before actual tests.

## Interactive Capabilities

The TCS provides the capabilities to interactively control a thermal test (ref. 3) by the operator such as ramp up, start, hold, resume, and stop. The operator can initiate a thermal test by selecting the ramp up or start function. The operator can hold a thermal test by selecting the hold function and can resume a thermal test by selecting the resume function. The operator can stop a thermal test at any time by selecting the stop function.

*Ramp Up*

During the ramp up, the TCS brings all zones to their first thermal setpoints and maintains these temperatures while waiting for thermal start to be initiated. For each active control TC, the ramp up temperature difference between its first thermal setpoint and its initial skin temperature is computed. The maximum ramp up temperature difference is determined by comparing all the ramp up temperature differences. The ramp up time is calculated through dividing the maximum ramp up temperature difference by the maximum ramp up rate defined in the PCM. From the ramp up time, the ramp up rate for each control TC is calculated via dividing the ramp up temperature difference by the ramp up time. In order for the first thermal setpoints to start at the Thermal Profile Elapsed Time (THRM PET) equal to zero, the ramp up time must be a negative number as displayed in the real-time temperature graphs. When the ramp up finishes, the TCS will inform the operator and maintain the first thermal setpoint for each zone at THRM PET equal to zero.

*Start*

If the ramp up had been selected and the TCS finished the ramp up, the TCS would start segment 1 immediately when the start function is selected. If only the start is selected, the TCS will go through the ramp up period described above. When the ramp up time is reached, the TCS starts segment 1 at THRM PET equal

to 0. For each control TC and each segment, the TCS uses the information in the PCM to compute thermal setpoints and to execute its tasks. When one segment ends, the next segment starts until the last segment is completed. During a thermal test, the TCS calculates the power level for all control TC every 200 ms until THRM PET is equal to the preplanned thermal profile time programmed in the PCM. When a thermal test finishes successfully, the TCS zeroes out all power level buffers, stops the thermal test, shut down all PCCs used in the test, and notifies the operator.

### Hold

After the ramp up or the start is selected, the hold function becomes available. When the hold is selected, the TCS holds each control TC profile temperature at the thermal hold time, and THRM PET is not increased until the resume function is selected.

### Resume

When the resume function is selected, the TCS resumes from where the hold function has been selected. THRM PET increases, and the profile temperatures continue from the thermal hold time.

### Stop

After the start or the ramp up function is selected, the stop function can be selected at any time during a thermal test. When the stop function is selected, the TCS zeroes out all power level buffers, stops the thermal test, shuts down all PCCs used in the test, and notifies the operator. There will be no firings and no options to go back to the thermal test from this point.

# Programmed Capabilities

There are additional TCS capabilities that are programmed in the thermal maps: limit checking, average power level, maximum power level, feedback temperature sensor switching, and replay power level.

### Limit Checking

The limit checking capability offers the option to shut down a thermal test in case any control TC temperature exceeds its predefined limits programmed in the CLM. There are four limits: highest temperature limit, lowest temperature limit, high deviation limit, and low deviation limit. The limits can be defined with any appropriate values based on each test. The highest temperature limit and the high deviation limit are for the overheated cases. The lowest temperature limit and the low deviation limit are for the underheated cases. In each segment, the information programmed in the PCM provides the TCS with which types of limit checking that must be performed.

### Average Power Level

The average power level capability provides the TCS a choice to either use the calculated power level or average it with previous power levels. This capability prevents sudden changes in power levels. In the PCM, there is an integer representing the number of previous cycles used in the average power level. If this integer equals to 0, the calculated power level is used. If this integer is a non-zero, an average power level is computed using 50 percent of the calculated power level and 50 percent of previous power levels specified by the integer.

### Maximum Power Level

The maximum power level capability allows putting a limit on the power level in each segment. If the calculated power level is greater than the programmed maximum power level in the PCM, it is reduced to the maximum power level. This capability helps to prevent overheating.

### Feedback Temperature Sensors Switching

The feedback temperature sensor switching capability provides switching from one feedback temperature sensor to another feedback temperature sensor in one zone. For example, with the thermal profile in Appendix E, zone 1 has two control TCs, CTC01 and CTC02. CTC01 is the feedback temperature sensor from segment 1 to segment 4. CTC02 is the feedback temperature sensor from segment 4 to segment 8. The TCS checks every segment to know when to switch the feedback temperature sensor.

### Replay Power Level

The replay power level capability allows running a thermal test with power levels recorded in a previous thermal test, and either continuing to closed-loop thermal control or finishing the test. The selected power level recorded file must be loaded into the ACP before starting the test. In the PCM, the switch time and the transition time must be programmed. When the thermal test starts, the power level recorded file is opened, and the power level data is read until non-zero power levels are found. Every cycle from here, the TCS compares THRM PET with the switch time. If THRM PET is less than the switch time, the TCS reads power levels from the recorded file and fires the heaters. After the switch time is reached, the TCS checks for the transition time. If the transition time equals to zero, the thermal test is done, and the TCS zeroes out all power level buffers, stops the thermal test, shuts down all PCCs used in the test, and notifies the operator. If the transition time is greater than zero, the TCS performs a transition from replay power level to closed-loop control and brings up all zones to their first profile temperatures during the transition time. After the transition period, the TCS automatically starts segment 1 of the thermal profiles and continues until the last segment.

## Pre-test Capabilities

After a thermal test setup is completed, some preliminary thermal tests must be conducted before running actual tests. Preliminary tests include lamp check, zone check, and SpecId. These tests help to avoid unnecessary failures during actual tests and contribute in saving time, resources, money, and maintaining on-time schedules.

### Lamp Check

The lamp check capability allows checking each individual output module (D/A) that is connected to its PCC channel and QL heater. Selecting an output module and selecting a current signal from 4 mA to 20 mA (normally 5 mA is used), an operator can fire the corresponding QL heater. If the corresponding QL heater doesn't fire as instructed, there must be a problem with either the output module or the associated PCC channel or the QL heater and the problem must be corrected.

### Zone Check

The zone check capability is used to verify the setup of each zone with its output module, PCC channel, QL heater, and control TC. Each zone is commanded with a very low power level in the range of 3 percent to 10 percent of full power; normally 3 percent is used. Test personnel with proper eye protection performs a visual check and verifies that the correct PCC channel and QL heater are fired. The zone control TC is checked and verified for rising temperature. This capability allows zones to be checked in any combination from one at a time to all zones at once.

### Specimen Identification

After the lamp check and the zone check, a SpecId test is run to determine *acoeff* and *bcoeff* coefficients. The SpecId was explained in detail in the integral gain coefficient, $K_i$, and proportional gain coefficient, $K_p$, section. A SpecId maximum temperature, a SpecId minimum temperature, and a very low SpecId power level for each zone are programmed in the thermal maps. When the SpecId test is complete, *acoeff* and *bcoeff* coefficients are calculated, recorded, and ready for use. These coefficients are used in the calculation of $K_i$

and $K_p$. If a test article or coupons were used in previous tests, the SpecId does not need to be run since the *acoeff* and *bcoeff* coefficients were already calculated.

## GRAPHITE HEATER CLOSED-LOOP THERMAL CONTROL

In 2005, the FLL purchased graphite heater PCCs with the objective to support heating tests with temperatures up to 3000 ºF. Each graphite heater PCC has a built-in TCS and can be used by itself to run only GH. On the other hand, the TCS can be used for only QL heaters. Therefore, to have both QL and GH synchronized in the same test, GH closed-loop thermal control was implemented in the TCS.

In 2006, the small test chamber was setup with two GH zones. The same thermal profile defined in Appendix E and shown in figure 15 was applied to both zones. Figure 16 displays the GH elements used in thermal tests. At the beginning, the derived QL thermal control equations were implemented for GH the same way as for QL. However, the QL thermal control equations did not work for GH. The real-time deviation and power level recorded data were studied and analyzed. The real-time graph in figure 17 shows a long delay and the cyclic pattern of overheating and underheating. At THRM PET equals to 200 s, the profile temperature is 530 ºF; the real-time graph in figure 17 shows the skin temperature is around 275 ºF, 255 ºF below the desired temperature. The test data confirms the sluggishness of the GH at the beginning of a test. It is found that when the system was underheated, the TCS produced high power levels in an effort to try catching up with the profile temperature; and when the profile temperature was caught up, it was soon overheated. Similarly, when the system was overheated, the TCS produced low power levels in an effort to try descending down to the profile temperature; and when the profile temperature was achieved, it was soon underheated. Since the GH elements have very high thermal inertia as compared to QL, these problems were expected.

The solution for the GH beginning sluggishness is to fire with high power levels for the first five seconds depending on the ramp up temperature difference between the first thermal setpoint and the ambient temperature. For the underheating problem, the current deviation must be in the range of 15 ºF to 0 ºF, and the deviations of the last three cycles must all be higher than the current deviation; the control logic decreases the power levels depending on the values of the current deviation. For the overheating problem, the current deviation must be in the range of -15 ºF to 0 ºF, and the deviations of the last three cycles must all be smaller than the current deviation; the control logic increases the power levels depending on the values of the current deviation. The extra software control logic was developed to handle the GH high thermal inertia. The real-time graph in figure 18 demonstrates that the GH closed-loop thermal control operates within the required range. At THRM PET equals to 200 s, the profile temperature is 530 ºF; the real-time graph in figure 18 shows the skin temperature is around 530 ºF, very close to the desired temperature.

The test setup was changed to one GH zone and one QL zone with the same previous thermal profile defined in Appendix E. The test results proved that the TCS new capability of combining QL and GH in a same test was achieved as shown in figure 19. At profile elapsed time equals to 200 s, the profile temperature is 530 ºF; the real-time graph in figure 19 shows the skin temperature is around 530 ºF, very close to the desired temperature. This combination test proves that the TCS can run with both QL and GH heaters in a same test.

## GRAPHITE HEATER OPEN-LOOP POWER LEVEL

Later, there was a need to have the GH open-loop power level capability to heat a test article with predefined power levels. With the new capability, the TCS can fire the GH with power levels from a time history power level profile predefined by the user in the PCM and with no ramp up period. The hold, resume, and maximum power level capabilities are required to be the same as the closed-loop thermal control. The control TC for each zone must also be installed for monitoring the zone temperature.

In the PCM, power level profiles replace temperature profiles. In each segment, there are start time, end time, slope in power levels/sec, intercept in power level, and other important information. For this test type, SpecId doesn't need to be run. Only the highest temperature limit check is available and must be enabled to ensure that the open-loop power level test doesn't run away from the predefined highest temperature limit, and burn the test article and/or the test setup.

During a test if the hold function is selected, each zone continues to fire with the same power level at the thermal hold time, and THRM PET is not increased. When the resume function is selected, THRM PET is increased, and the power level profiles continue from the thermal hold time.

A small test chamber with one zone of GH was used to develop this new capability. Verification and validation for the open-loop power level capability are accomplished by verifying the power levels in the recorded file with the predefined time history power level profile.

The GH open-loop power level capability was utilized to heat a ceramic matrix composite (CMC) panel with preplanned power levels programmed in the PCM. The hold function was selected during a test to fire the GH at a certain power level for a period of time before returning back to the power level profile. There was also a test where the CMC panel was heated using the maximum power level of 12. All of these tests were conducted to study how fast the temperatures rise for different power levels. The highest limit check is always used in these tests to ensure that the test article and/or the test setup will not be overheated above the permitted temperature. When the temperature reached its highest temperature limit, the TCS would stop the test immediately to prevent any damages from occurring.

# LARGE-SCALE HEATING TESTS

For almost a decade, this in-house PI TCS has fulfilled its responsibility to support large-scale heating tests in the FLL. All large-scale tests were accomplished in a large test chamber with high number of zones and large test articles. The TCS successfully met the test objectives defined for each test. The test data were used by researchers and engineers to evaluate the performance of the hot structures in the tests.

The C/C control surface tests were the first QL large-scale heating tests that used the PI TCS (fig. 14). The carbon-silicon carbide (C/SiC) hot structure subcomponent tests were soon followed successfully. The above tests were the first combined thermal/mechanical tests performed on CMC hot structures. A series of QL thermal and thermal/mechanical tests were completed on other hot structures which included both C/SiC and C/C subcomponents. The combined QL_GH thermal tests were executed on a test article where some GH zones achieved temperatures up to 3000 ºF; the highest temperature ever accomplished by the PI TCS.

# THERMAL CONTROL SYSTEM DISCUSSION

In this section, real-time graphs and test data of a typical CMC hot structure test are used to highlight the performance of the TCS. This thermal test has 18 QL zones, and the thermal profile time programmed in the PCM is 1900 s. Zones 2, 10, 12, and 13 are selected for the discussion.

THRM PET in figure 20 displays 1706 s, 194 s short of the thermal profile time programmed in the PCM. The termination was caused by the high deviation limit of CTC34 (Zone 10) at THRM PET equal to 1706 s. The TCS stopped the thermal test, zeroed out all power level buffers, shutdown all PCCs used in the test, and informed the operator of the cause of the shutdown. The thermal test had stopped, but the test data recording went on until the test article cooled down to a safe temperature range; therefore, the real-time graphs continued. After the test stopped, the deviation and the power level recorded files were downloaded and analyzed. From the deviation data as shown in figure 21a, the shutdown of high deviation limit was verified and validated. At THRM PET equal to 1706 s and test time equal to 6622 s (fig. 20), CTC34 absolute value

of temperature deviation was 300.90 ºF, just over the predefined high-deviation limit of 300.0 ºF in the CLM. The TCS shutdown the thermal test instantly at the first time the high-deviation limit occurs. From the power level data shown in figure 21b, the power level went to zero at THRM PET equal to 1600 s and test time equal to 6516 s (fig. 20) which was 106 s before shutdown. Therefore, even without power for the last 106 s before shutdown, the CTC34 remained at much higher temperatures than the preplanned profile temperatures and caused the high-deviation limit shutdown. Overheating during the cool down phase with negative slopes (-5.81 ºF/s for CTC33 and -5.31 ºF/s for CTC34) happens often in test setups not incorporate with an active cooling system. Actually many other control TCs would exceed high-deviation limits if CTC34 did not.

After the thermal test is terminated, figure 22 shows that the thermocouple junction of CTC39 (Zone 2) opened, and its temperature jumped over 3200 ºF at test time equal to 6675 s. This real-time display provided the test team visual information that CTC39 must be fixed before the next test.

CTC15 (Zone 12) and CTC16 (Zone 13) had the same thermal profile. Zone 12 and Zone 13 real-time graphs in figure 23 were overlapped, and it is impossible to distinguish them during the heating phase. Only during the cooling phase, the two graphs started to separate at THRM PET equal to 1630 s and test time equal to 6546 s. The graphs of the preplanned thermal profiles for CTC14, CTC15, and CTC16 are shown in figure 24. In order to compare the real-time graphs and the preplanned thermal profiles, the ramp up time and the first segment start time are mentioned. From the test data, ramp up started at THRM PET equal to -43 s and test time equal to 4873 s, and segment 1 started at THRM PET equal to 0 s and test time equal to 4916 s (fig. 23). The graphs of real-time deviation and power level for Zone 12 are in figure 25, and the graphs of real-time deviation and power level for Zone 13 are in figure 26. Even Zone 12 and Zone 13 real-time temperature graphs were inseparable, the deviations and power levels were different at all times. For Zone 12, the CTC15 deviations as shown in figure 25a were still in good operating range, and Zone 12 power levels as shown in figure 25b were very small but non-zeroes at THRM PET equal to 1630 s and test time equal to 6546 s (fig. 23). For Zone 13, the CTC16 deviations as shown in figure 26a started to be negative and continued increasing more negative, and Zone 13 power levels as shown in figure 26b had already been zeroes at THRM PET equal to 1630 s. The above discussion explains why Zone 12 and Zone 13 real-time graphs started to separate from each other during the cooling phase with no power present.

The deviation and power level graphs demonstrate that at the beginning, the QL thermal control is very oscillatory at low temperatures and low power levels with more off cycles. When a quartz lamp is fired, its control TC temperature increases; and when the quartz lamp is off, its control TC temperature decreases. The control becomes much better at higher temperatures and higher power levels with more on cycles. Since this TCS does not have an active cooling system, one of the zones with negative slopes during the cooling phase normally triggers the shutdown due to exceeding high deviation limit. Even with no power, all zones retain so much heat causing the control TC temperatures to be too high compared to the corresponding profile temperatures.

For all thermal tests, the construction of a zone, and the positions of control TC and heater are very important with respect to the performance of the TCS. If a zone is insulated well, and the control TC is positioned near the heater; the control is very good, and the errors can achieve ±0.5 °F. If a zone is insulated poorly, and/or the control TC is positioned not well; the control can become oscillatory, and the errors can reach ±20.0 °F.

## CONCLUDING REMARKS

The PI thermal control system described in this paper is a very reliable, safe, and robust system that was built in-house to support thermal testing in the FLL. The derived QL thermal control equations and algorithm are implemented with ANSI C in the ACP, a component of the existing DACS. The ACP calculates power

levels every 200 ms and sends current signals to the PCCs to fire QL and/or GH heaters to heat up a test article following preplanned thermal profiles.

From 2003 until 2010, the PI thermal control system has performed many thermal tests as described in the Large-Scale Heating Tests section. There are significant advantages in having an in-house thermal control system. When new requirements come up, new software and new test setups can be developed, tested, verified, and validated quickly. The GH closed-loop thermal control and GH open-loop power level are added later to satisfy the demand of higher temperature tests (up to 3000 ºF). Also, when a thermal test fails, the deviation and the power level recorded files can be used to analyze the causes of the problems, and the software fixes can be fast, helping the projects to stay on schedule.

Theoretically, equation (9) is the general PI control equation that can be used to build any control system with $R$ as the reference input, $C$ as the controlled variable, $E = R - C$ as the difference between $R$ and $C$, and $U$ as the controller output. An appropriate continuous-time mathematical model for the controlled process similar to the heating process must be defined between the controlled variable $C$ and the controller output $U$. Then, the continuous-time controlled process equation must be transformed to the discrete-time controlled process equation. The $U$ in the controlled process equation is replaced with the $U$ in equation (9) to develop the relationship between $C$ and $R$ from which the transfer function C(z)/R(z) in the $z$-domain is derived. For the system stability, the poles of the transfer function should be assigned on the real axis in the right-hand side inside the unit circle ($0.0 < z_1, \ldots z_i < 1.0$) to simplify the mathematical process. From the derivation of the transfer function and the controlled process equation, a stability region of the control system can be determined. The values of $K_i$ and $K_p$ should be tuned and selected carefully so that the control system is stable and robust. Besides the derived control equations, the control algorithm should always have capabilities similar to the ones described in the Thermal Control System Capabilities section such as reference input limit checking, and average and maximum controller output value to make the control system more safe and versatile.

# FIGURES
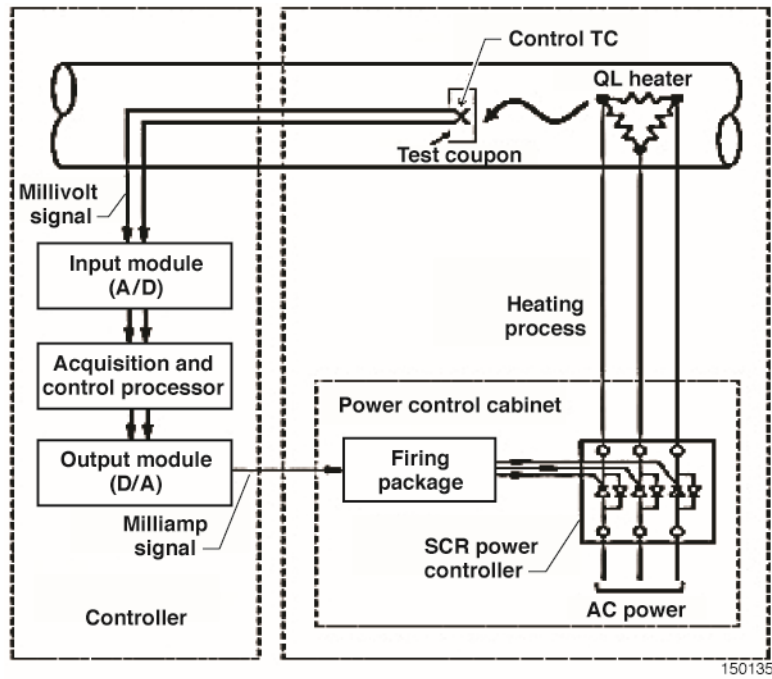


Figure 1. A quartz lamp thermal control system block diagram.
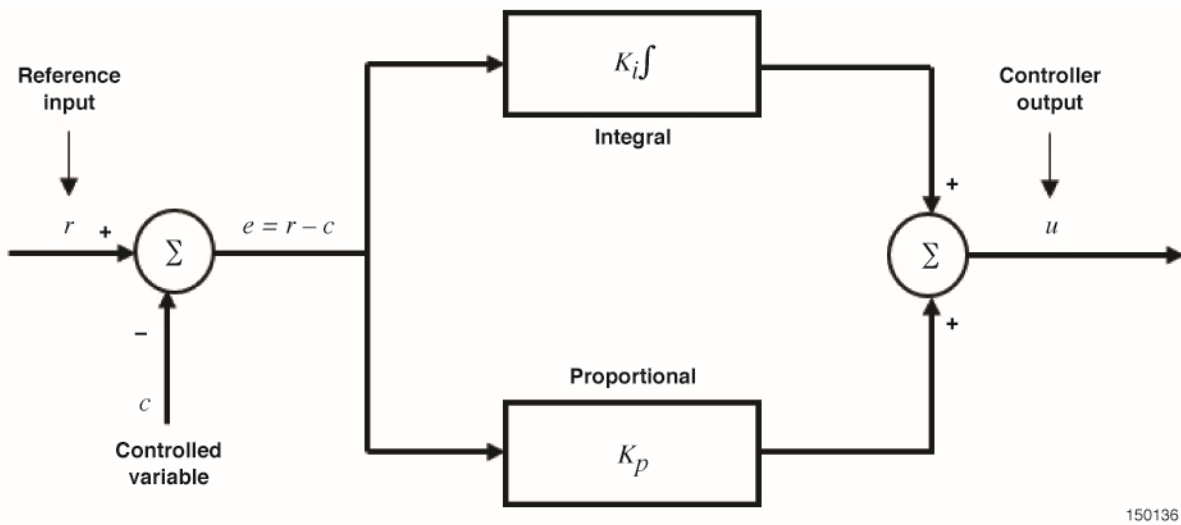


Figure 2. Proportional integral controller block diagram.
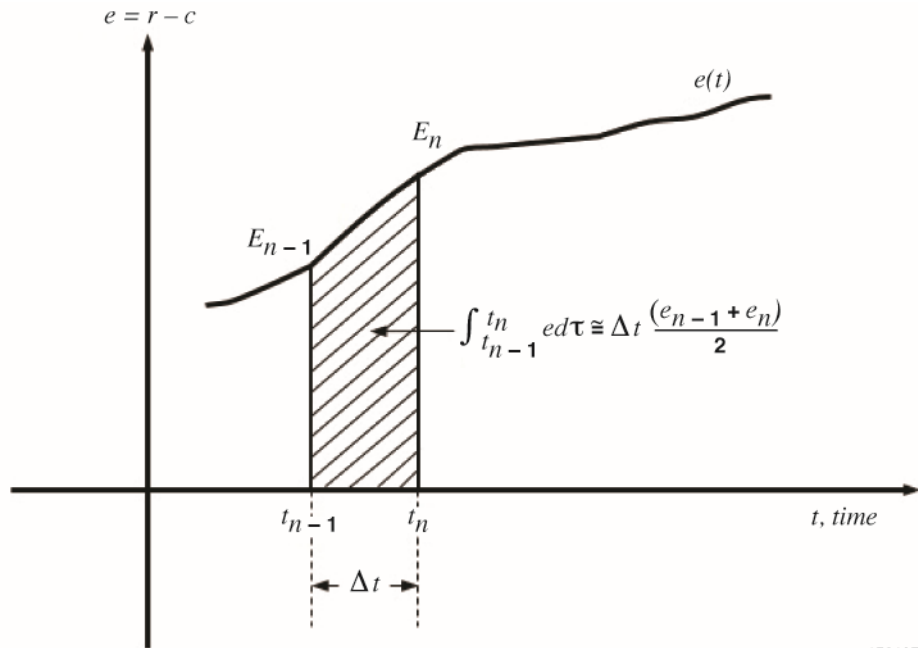
Figure 3. The integral of $e = r - c$ in $\Delta t = t_n - t_{n-1}$.
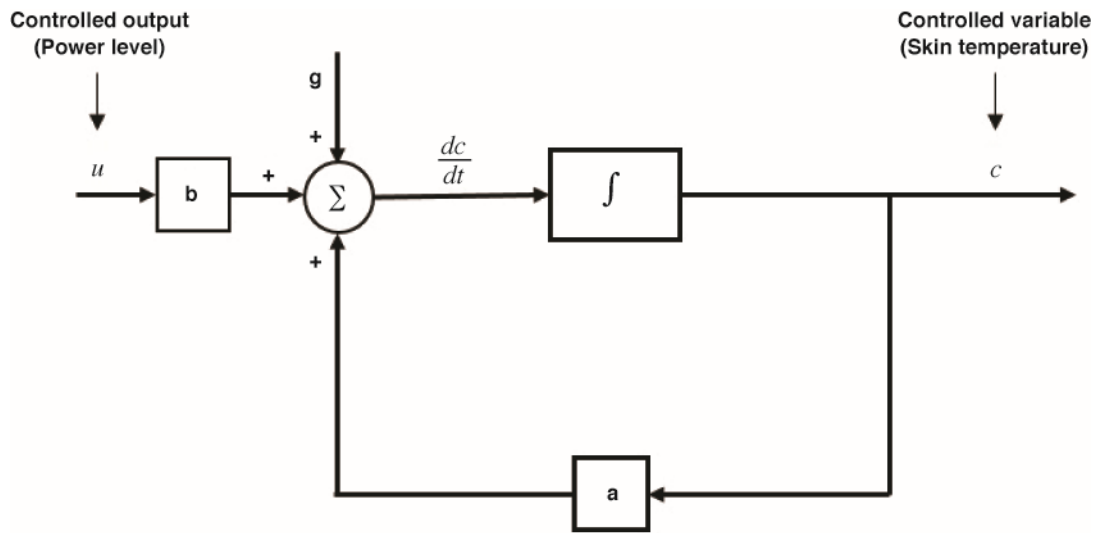


Figure 4. Heating process model block diagram.

22
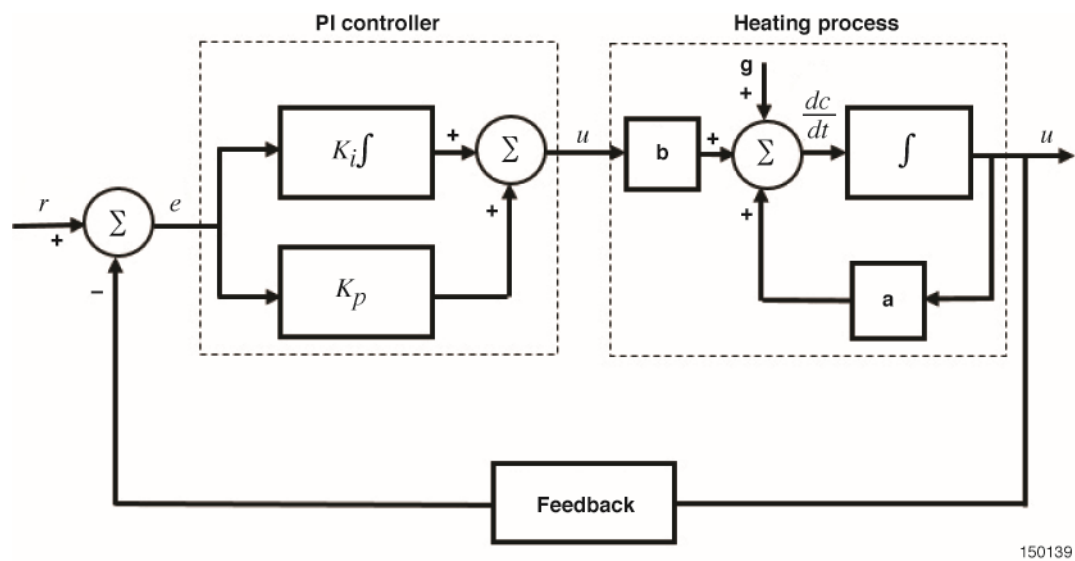
Figure 5. Closed-loop PI thermal control system block diagram.
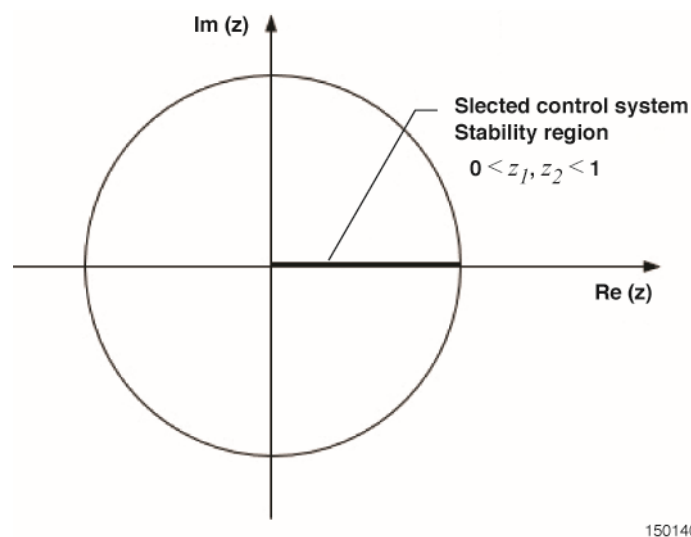


Figure 6. Selected control system stability region in the z-domain.
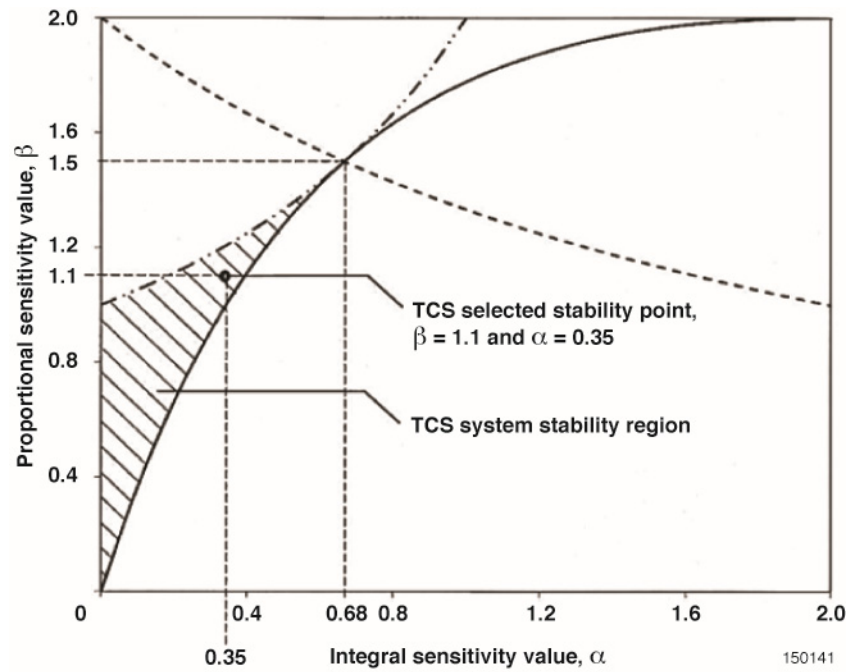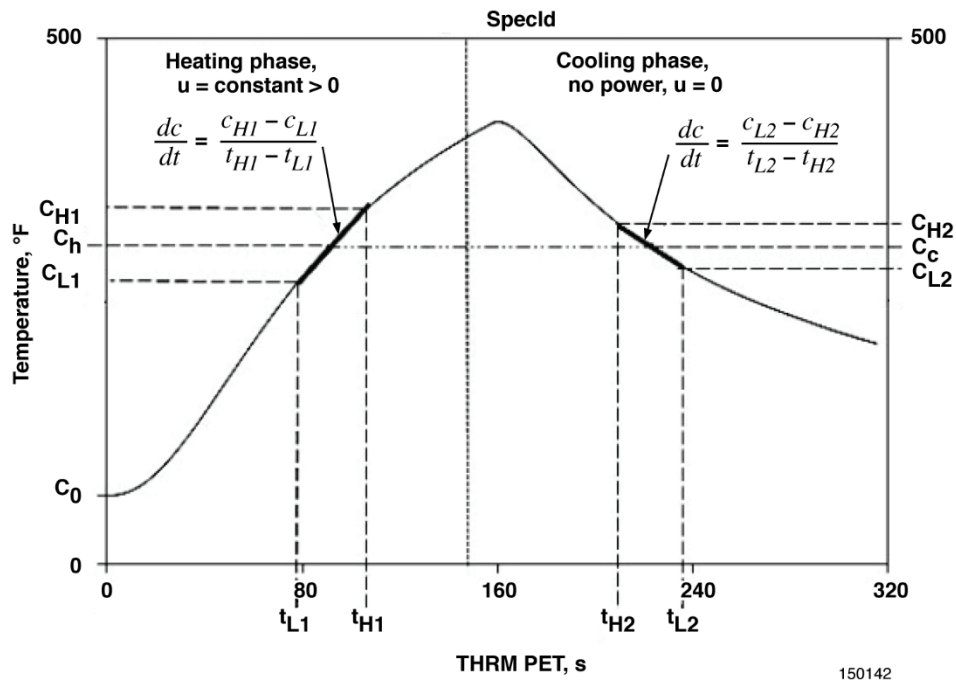
Figure 7. The PI thermal control system stability region.



Figure 8. Determination *acoeff* and *bcoeff* coefficients during SpecId.

24
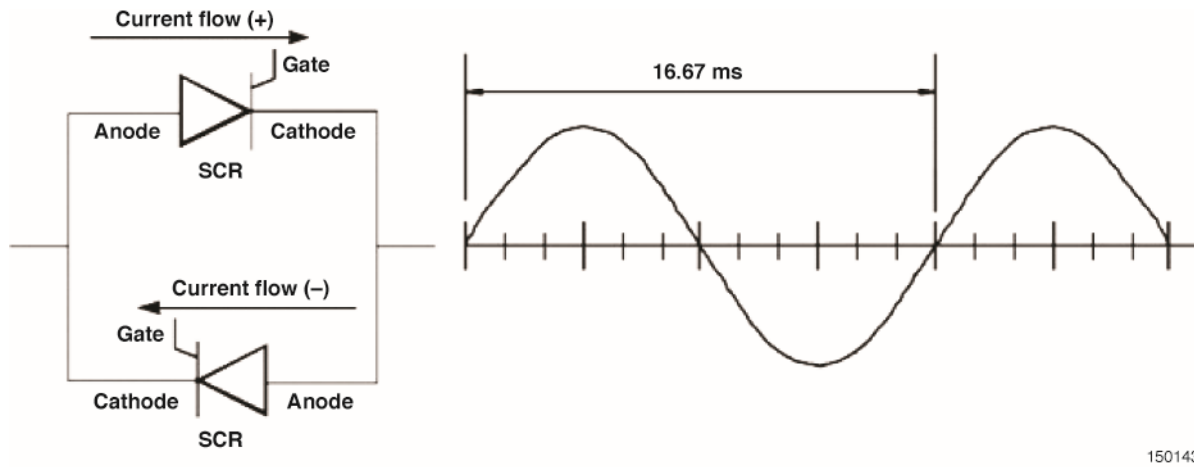
Figure 9. The power controller back-to-back silicon controlled rectifier configuration.
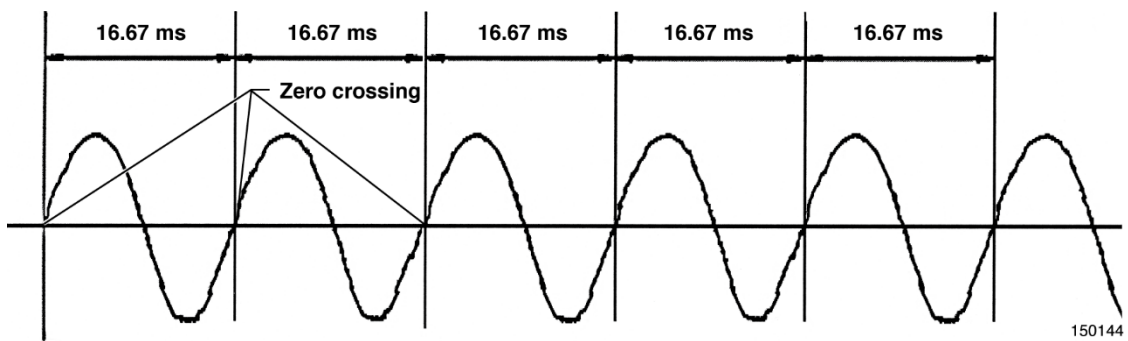


Figure 10a. 100 percent of full power firing, all cycles on.
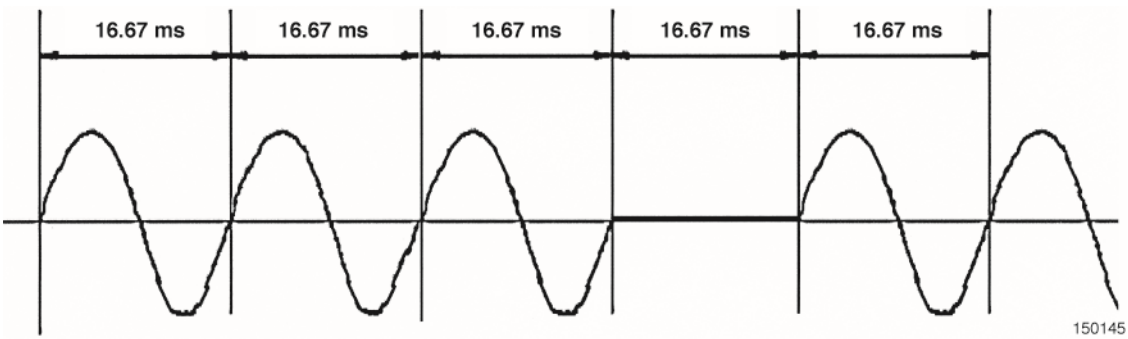


Figure 10b. 75 percent of full power firing, 3 cycles on and 1 cycle off.

Figure 10. Relationship between percentages of full power and number of cycles on/off.
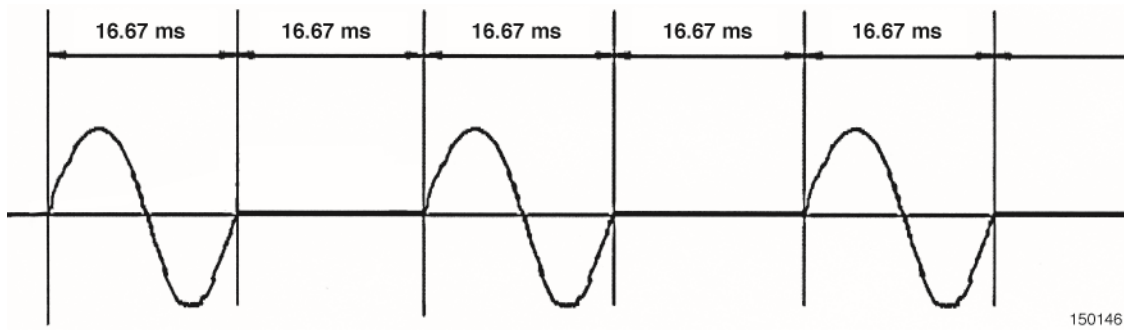
Figure 10c. 50 percent of full power, 1 cycle on and 1 cycle off.

Figure 10. Concluded.
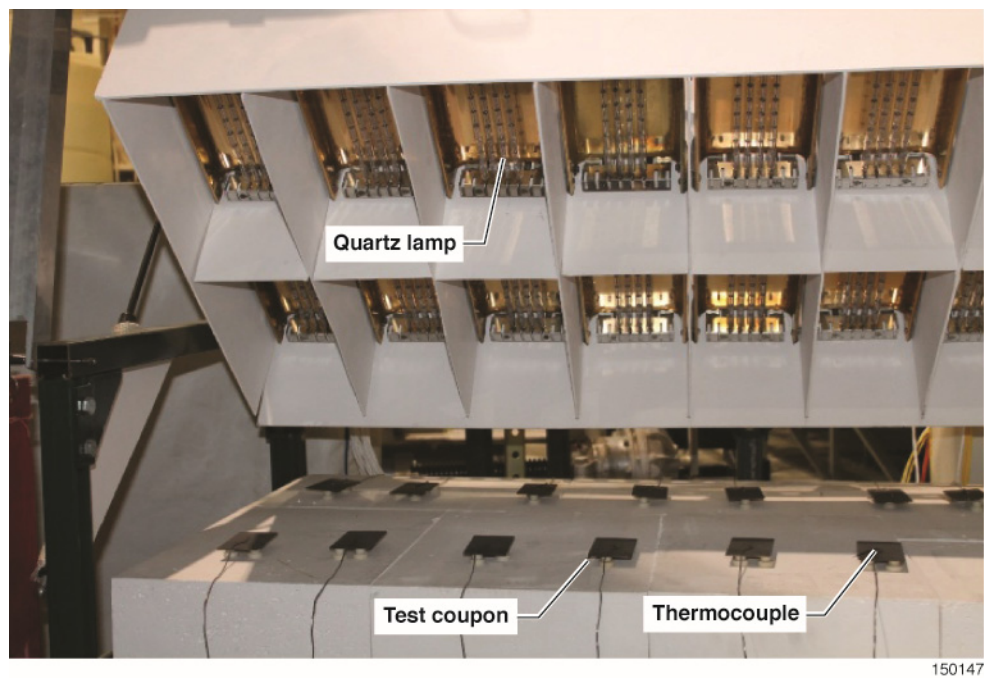


Figure 11. A multi-zone quartz lamp heater test setup.
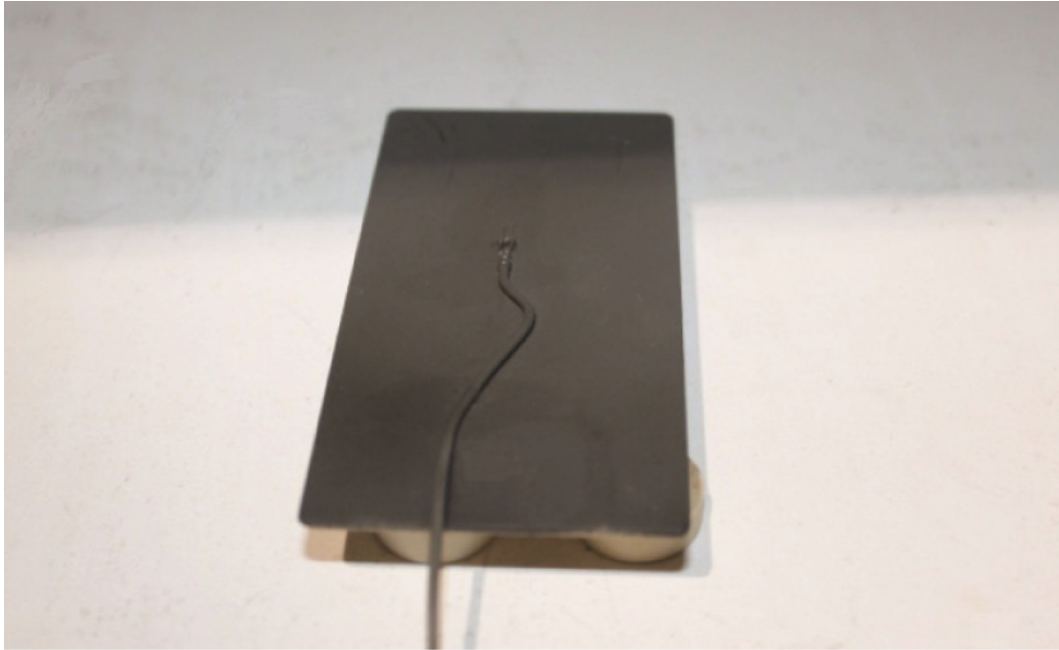
Figure 12. A typical control thermocouple attached on top of a test coupon.
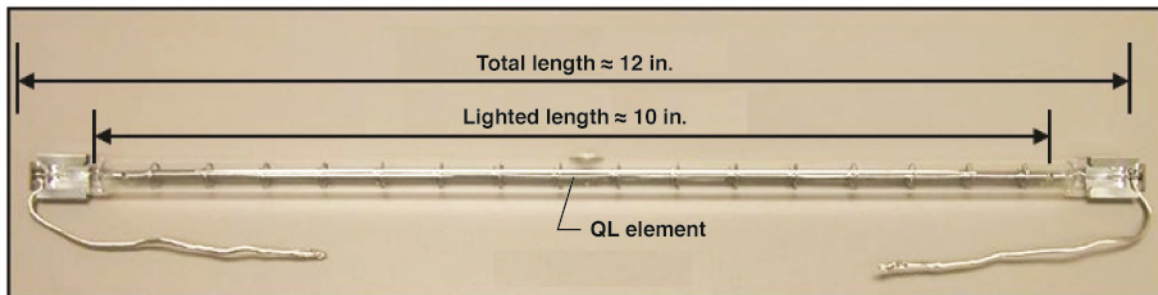


Figure 13. A typical single quartz lamp bulb.
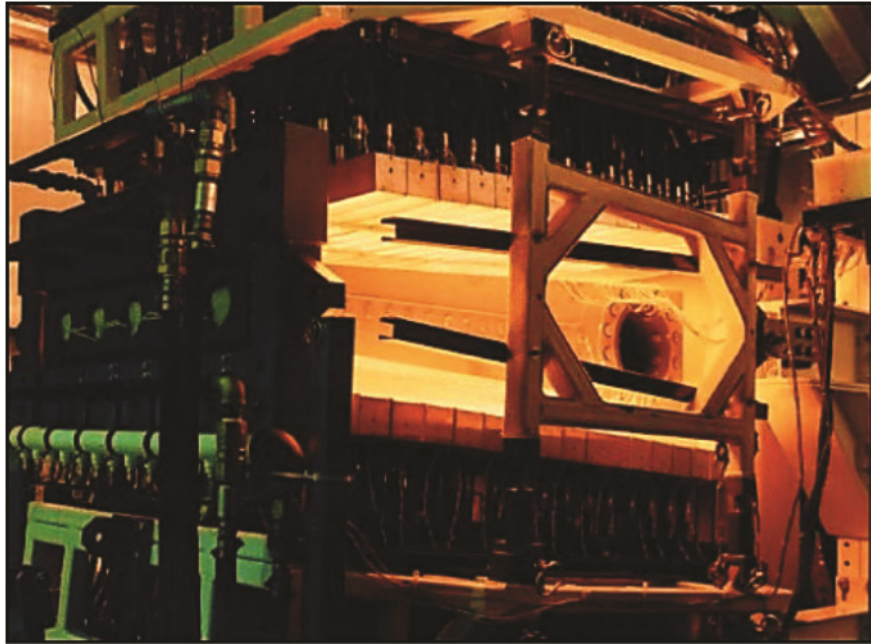
Figure 14. A QL C/C elevon large-scale heating test in the FLL.
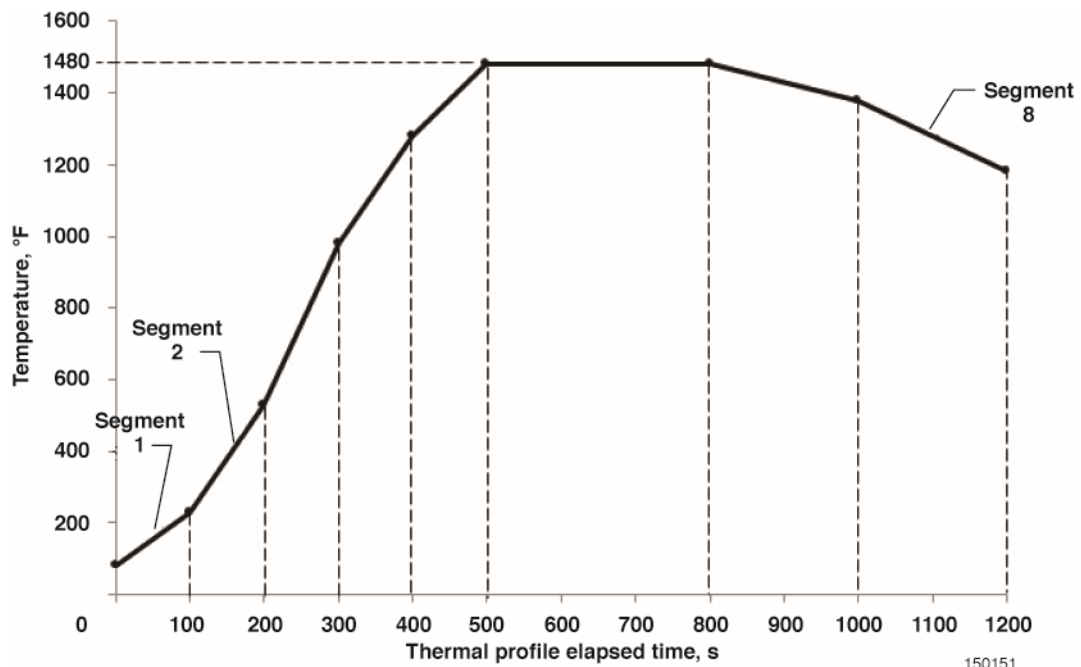


Figure 15. Graph of the thermal profile described in Appendix E.
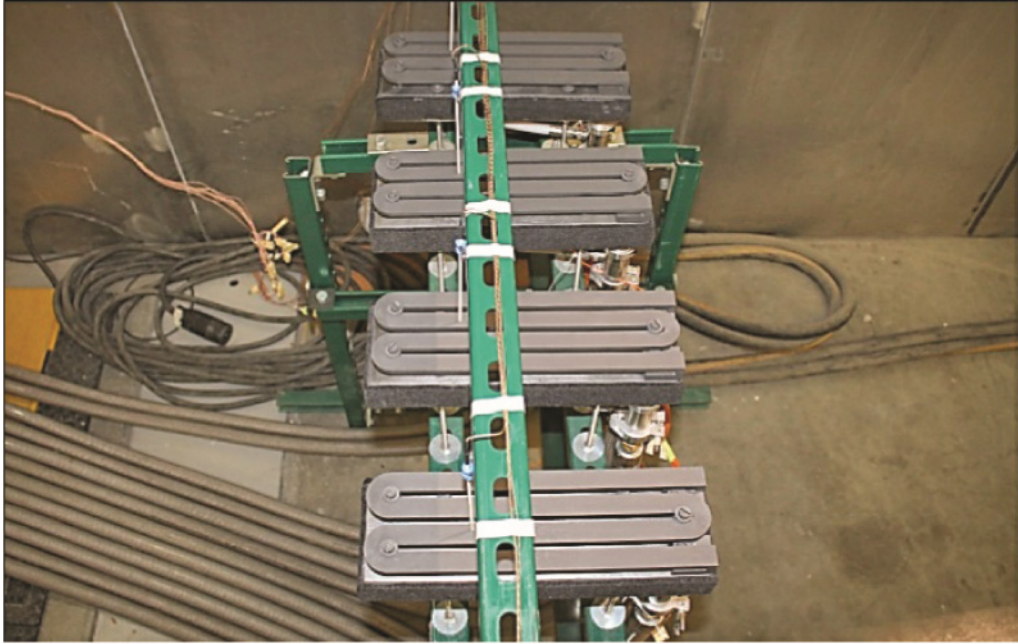
150152

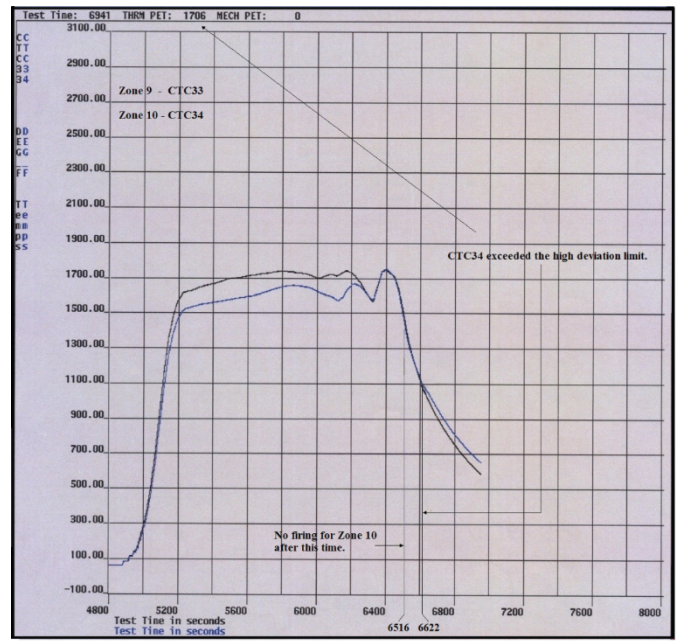Figure 16. Graphite heater elements.
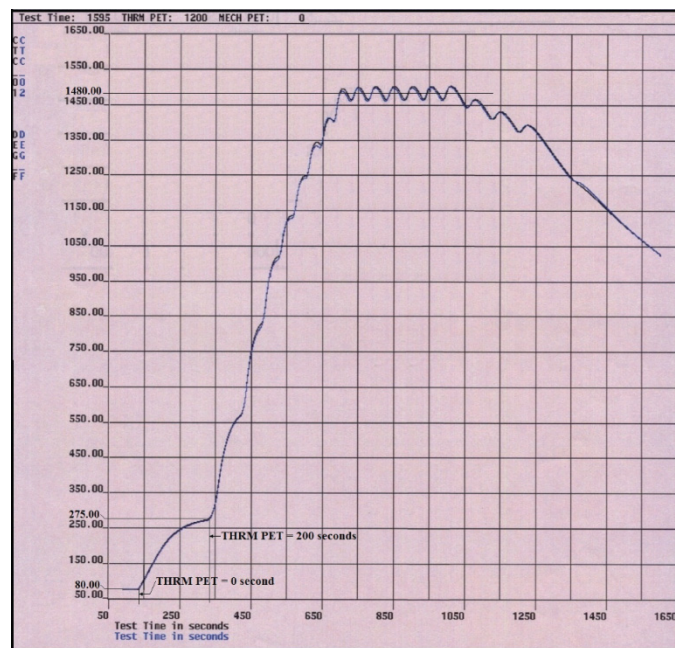


150153

Figure 17. Real-time temperature graphs of two GH zones.
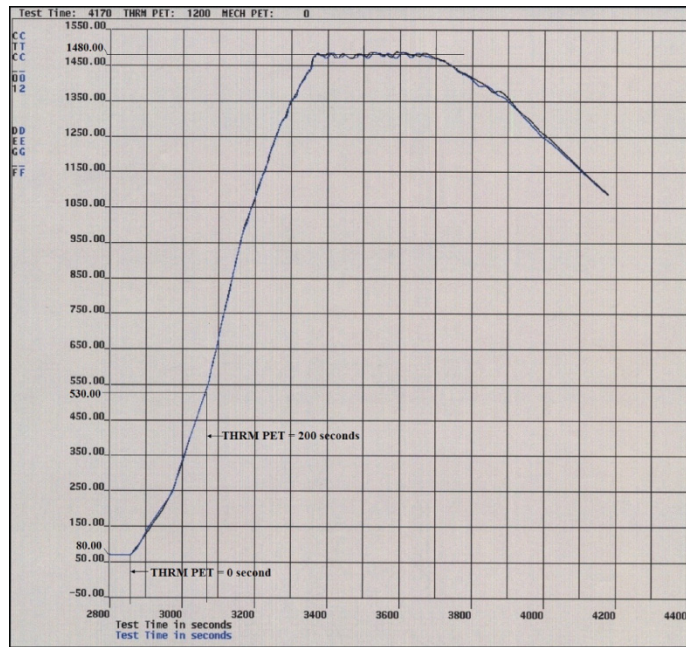
Figure 18. Real-time temperature graphs of two GH zones with control logic software.
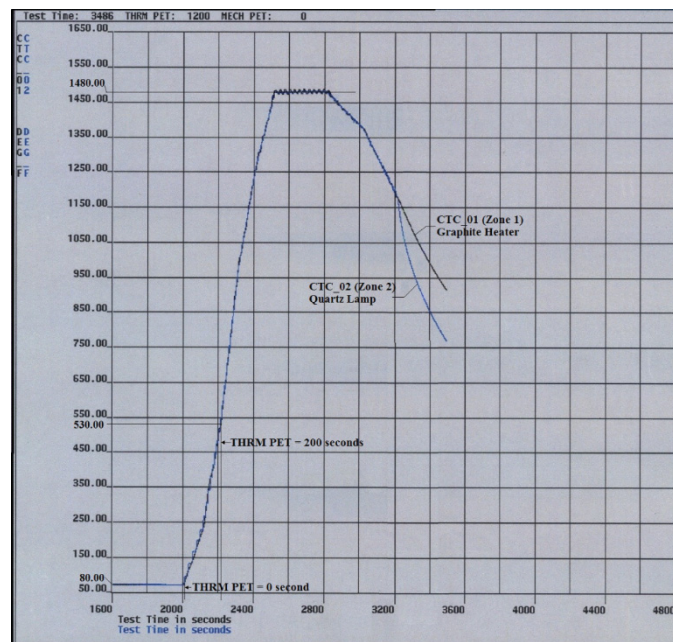


Figure 19. Real-time temperature graphs of one GH zone and one QL zone.
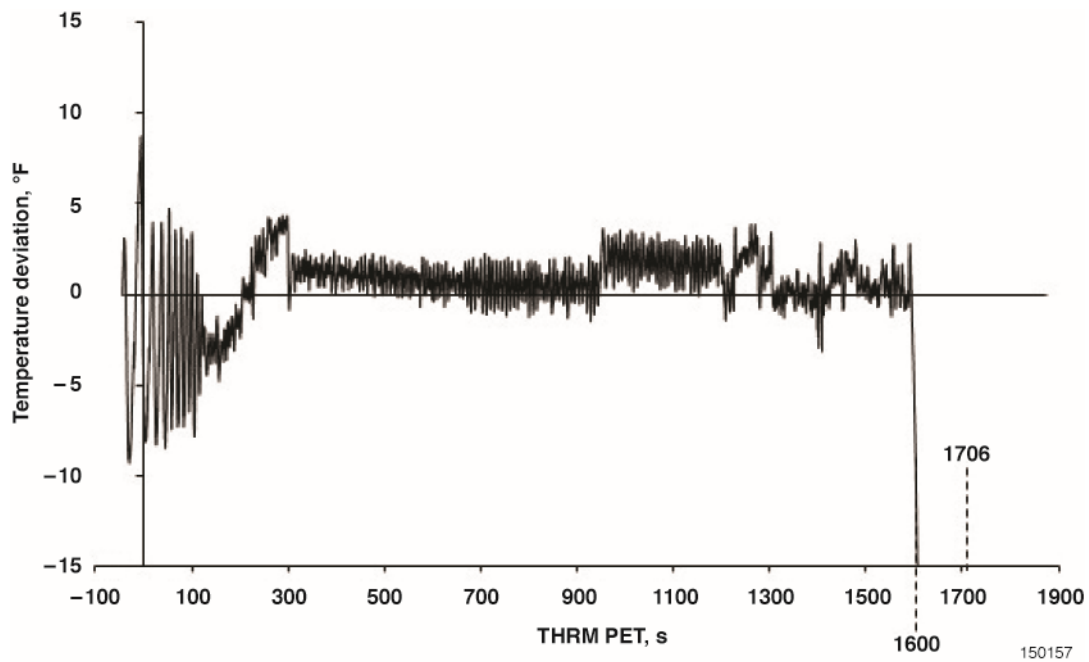
Figure 20. Real-time temperature graphs of Zone 9 and Zone 10.



Figure 21a. Real-time graph of temperature deviation.

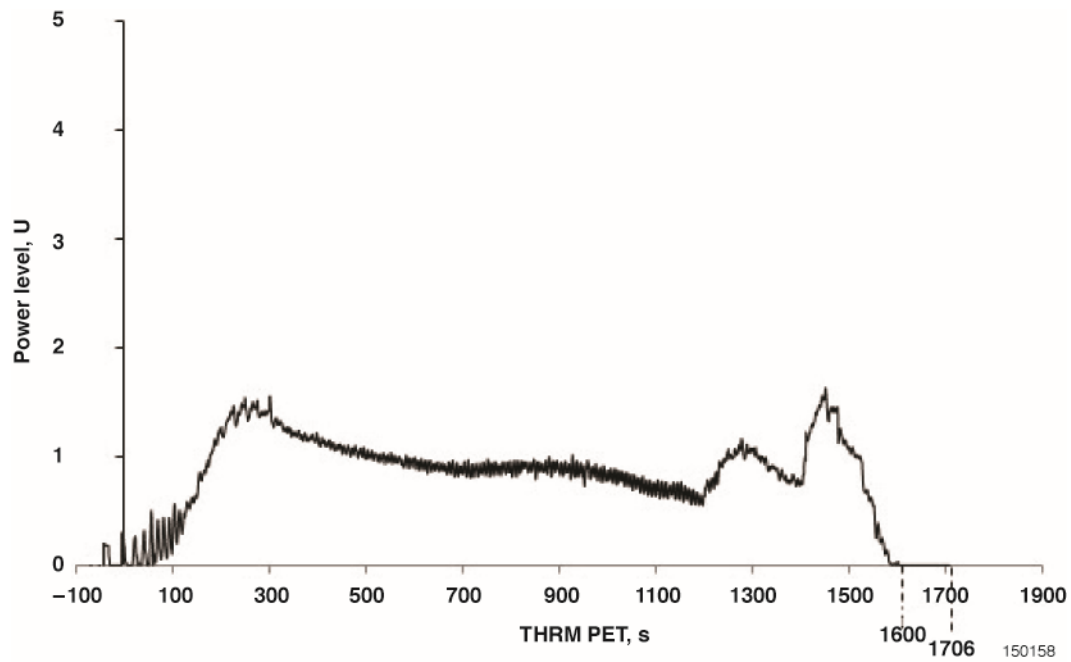Figure 21. Real-time graphs of temperature deviation and power level for CTC34, Zone 10.

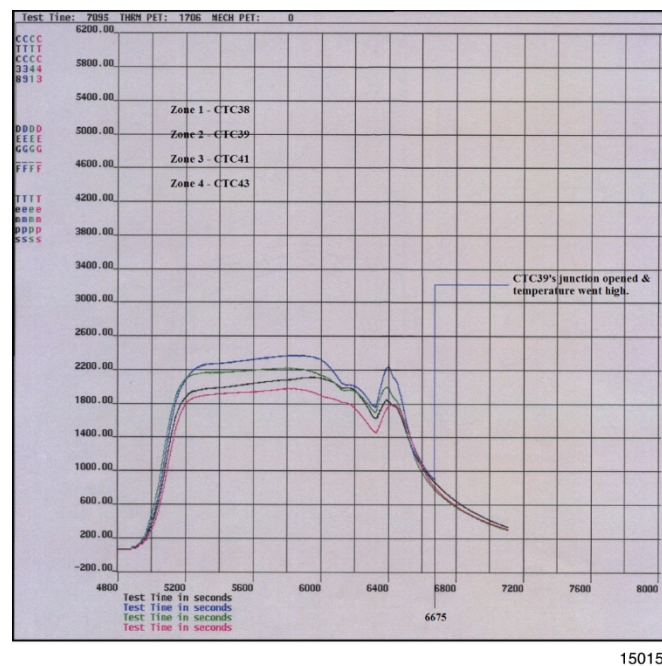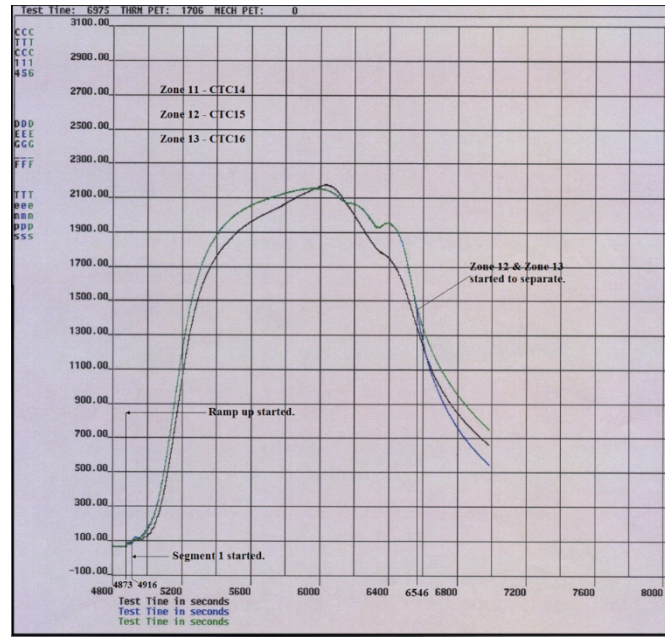Figure 21b. Real-time graph of power level.
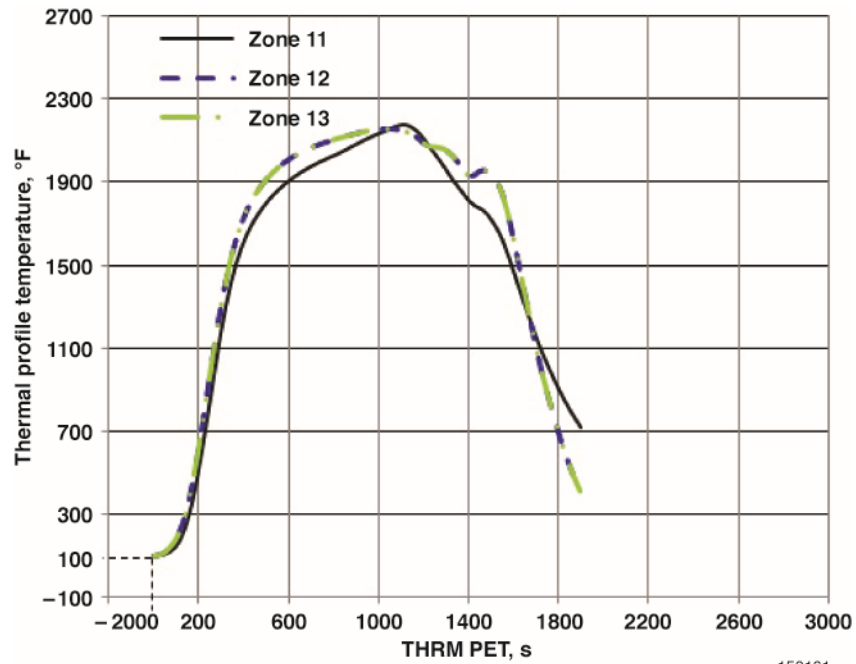
Figure 21. Concluded.



Figure 22. Real-time temperature graphs of Zone 1, Zone 2, Zone 3, and Zone 4.

Figure 23. Real-time temperature graphs of Zone 11, Zone 12, and Zone 13.



Figure 24. Preplanned thermal profiles of Zone 11, Zone 12, and Zone 13.

Figure 25a. Real-time graph of temperature deviation.



Figure 25b. Real-time graph of power level.

Figure 25. Real-time graphs of temperature deviation and power level for CTC15, Zone 12.
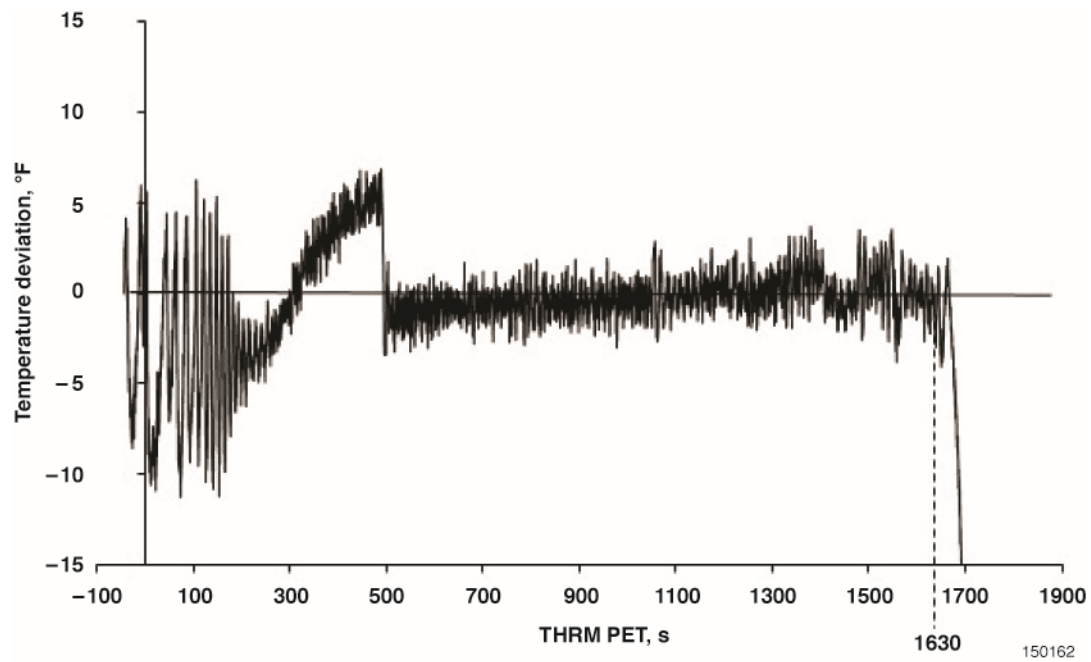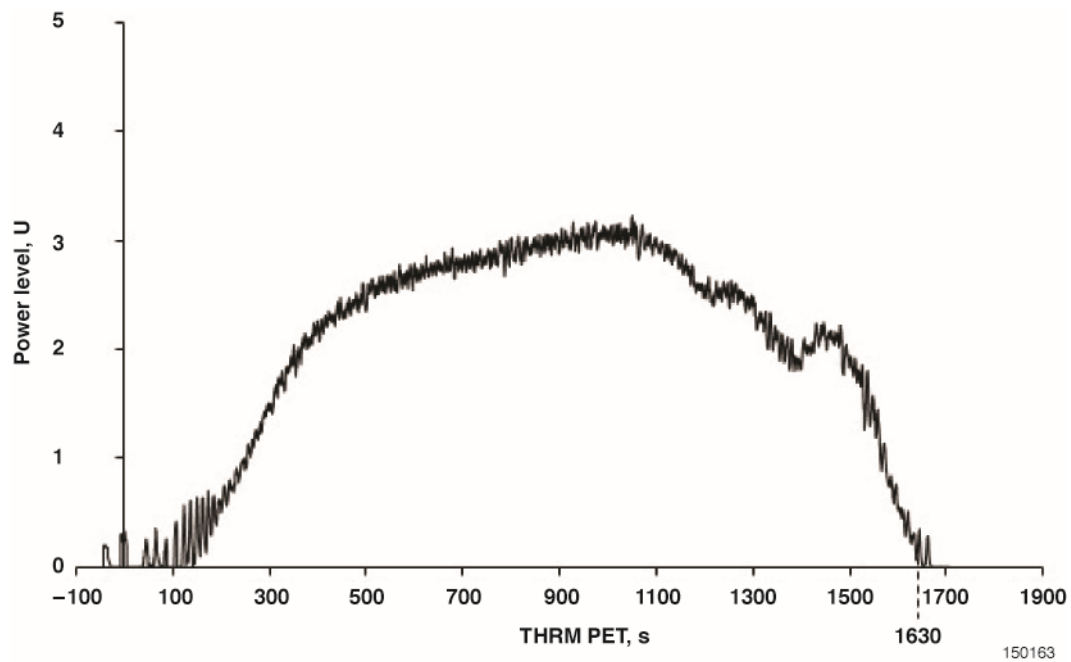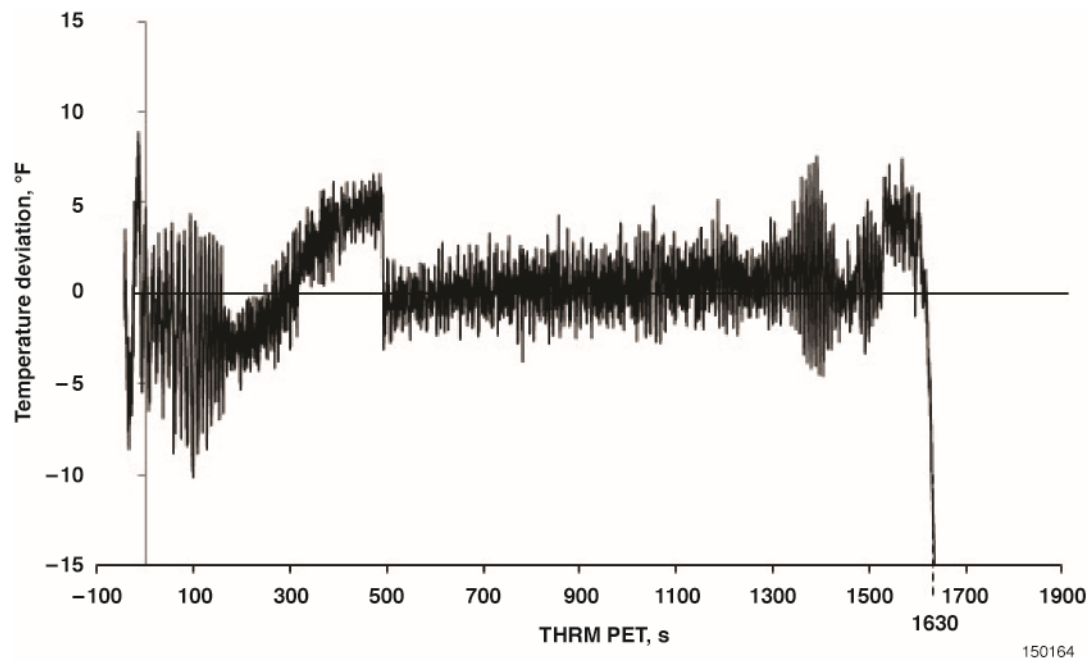
34

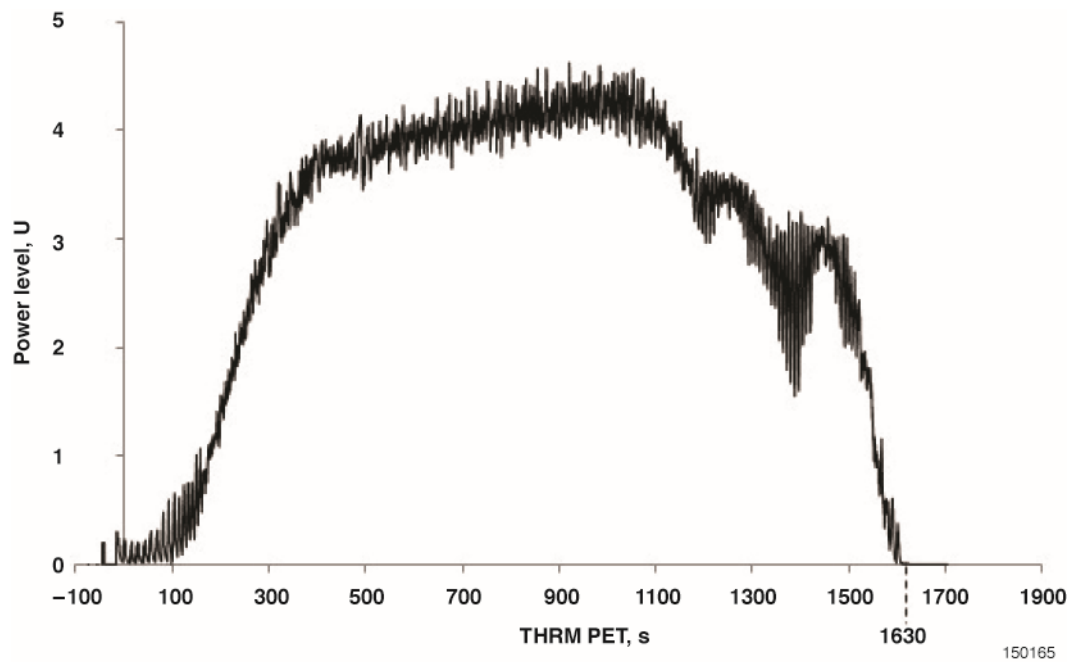Figure 26a. Real-time graph of temperature deviation.



Figure 26b. Real-time graph of power level.

Figure 26. Real-time graphs of temperature deviation and power level for CTC16, Zone 13.

# APPENDIX A
## Derivation of PI Controller Output

In this appendix, the discrete PI control equation (6) is written as equation (A1):

$$U_n = U_{n-1} + K_i \frac{\Delta t}{2}(E_n + E_{n-1}) + K_p(E_n - E_{n-1}) \tag{A1}$$

At time $n = 0$, equation (A1) becomes equation (A2):

$$U_0 \qquad (U_0 = 0) \tag{A2}$$

At time $n = 1$, equation (A1) becomes equation (A3):

$$U_1 = U_0 + K_i \frac{\Delta t}{2}(E_1 + E_0) + K_p(E_1 - E_0) \tag{A3}$$

Equation (A3) can be re-written as equation (A4):

$$U_1 = U_0 + K_i \frac{\Delta t}{2}[2(E_1 + E_0) - E_1 - E_0] + K_p(E_1 - E_0) \tag{A4}$$

At time $n = 2$, equation (A1) becomes equation (A5):

$$U_2 = U_1 + K_i \frac{\Delta t}{2}(E_2 + E_1) + K_p(E_2 - E_1) \tag{A5}$$

Replace $U_1$ in equation (A4) into equation (A5), and equation (A6) is achieved:

$$U_2 = U_0 + K_i \frac{\Delta t}{2}[2(E_1 + E_0) - E_1 - E_0] + K_p(E_1 - E_0) +$$
$$K_i \frac{\Delta t}{2}(E_2 + E_1) + K_p(E_2 - E_1) \tag{A6}$$

Expand and combine the like terms in equation (A6), and equations (A7) and (A8) are derived:

$$U_2 = U_0 + K_i \frac{\Delta t}{2}[2E_1 + 2E_0 - E_1 - E_0 + E_2 + E_1] +$$
$$K_p(E_1 - E_0 + E_2 - E_1) \tag{A7}$$

$$U_2 = U_0 + K_i \frac{\Delta t}{2}[2(E_2 + E_1 + E_0) - E_2 - E_0] + K_p(E_2 - E_0) \tag{A8}$$

At time $n = 3$, equation (A1) becomes equation (A9):

$$U_3 = U_2 + K_i \frac{\Delta t}{2}(E_3 + E_2) + K_p(E_3 - E_2)$$ (A9)

Replace $U_2$ in equation (A8) into equation (A9), and equation (A10) is achieved:

$$U_3 = U_0 + K_i \frac{\Delta t}{2}[2(E_2 + E_1 + E_0) - E_2 - E_0] + K_p(E_2 - E_0) +$$
$$K_i \frac{\Delta t}{2}(E_3 + E_2) + K_p(E_3 - E_2)$$ (A10)

Expand and combine the like terms in equation (A10), and equations (A11) and (A12) are derived:

$$U_3 = U_0 + K_i \frac{\Delta t}{2}[2(E_2 + E_1 + E_0) - E_2 - E_0 + E_3 + E_2] +$$
$$K_p(E_2 - E_0 + E_3 - E_2)$$ (A11)

$$U_3 = U_0 + K_i \frac{\Delta t}{2}[2(E_3 + E_2 + E_1 + E_0) - E_3 - E_0] +$$
$$K_p(E_3 - E_0)$$ (A12)

From the above expansion of equation (A1) for $n = 0, 1, 2, 3$, a general equation for the controller output power level $U_n$ at time $n$ is derived and shown in equation (A13):

$$U_n = U_0 + K_i \frac{\Delta t}{2}\left[\left(2\sum_{j=0}^{n} E_j\right) - E_n - E_0\right] + K_p(E_n - E_0)$$ (A13)

Moving the factor $\frac{1}{2}$ into the bracket [ ] and combining $E_n$ and $E_0$ term, equation (A14) is obtained:

$$U_n = U_0 + K_i \Delta t\left[\sum_{j=0}^{n} E_j - \frac{(E_n + E_0)}{2}\right] + K_p(E_n - E_0)$$ (A14)

Equation (A14) is the form of the power level at time $n$ for the time interval $\Delta t$.

# APPENDIX B
## Relationship between Controlled Variable and Reference Input

In this appendix, the discrete heating process equation (21) is written as equation (B1).

$$C_{n+1} = A(C_n - C_0) + BU_n + C_0 \tag{B1}$$

$\Delta t$ in the heating process was assumed to be the same as $\Delta t$ in the control model.
The discrete PI control equation (A13) was developed in Appendix A.

$$U_n = U_0 + K_i \frac{\Delta t}{2}\left[\left(2\sum_{j=0}^{n} E_j\right) - E_n - E_0\right] + K_p(E_n - E_0) \tag{A13}$$

Replace equation (A13) above into equation (B1), and equation (B2) is achieved:

$$C_{n+1} = A(C_n - C_0) + BU_0 + BK_i \frac{\Delta t}{2}\left[\left(2\sum_{j=0}^{n} E_j\right) - E_n - E_0\right] + \\ BK_p(E_n - E_0) + C_0 \tag{B2}$$

Replace $U_0 = 0$ and $E_n = R_n - C_n$ in equation (B2), and equation (B3) is derived:

$$\begin{aligned}
C_{n+1} = \;\; & AC_n - AC_0 + \\
& + BK_i\Delta t\left(\sum_{j=0}^{n} R_j - \sum_{j=0}^{n} C_j\right) - BK_i \frac{\Delta t}{2}R_n + BK_i \frac{\Delta t}{2}C_n \\
& - BK_i \frac{\Delta t}{2}R_0 + BK_i \frac{\Delta t}{2}C_0 \\
& + BK_p R_n - BK_p C_n - BK_p R_0 + BK_p C_0 \\
& + C_0
\end{aligned} \tag{B3}$$

Combine the similar terms of $C_{n+1}$, $C_n$, and $R_n$ in equation (B3), and equation (B4) is obtained:

$$\begin{aligned}
C_{n+1} = \;\; & C_n\left(A + BK_i \frac{\Delta t}{2} - BK_p\right) + R_n\left(BK_p - BK_i \frac{\Delta t}{2}\right) \\
& + BK_i\Delta t\left(\sum_{j=0}^{n} R_j - \sum_{j=0}^{n} C_j\right) \\
& + \left(C_0 - AC_0 - BK_i \frac{\Delta t}{2}R_0 + BK_i \frac{\Delta t}{2}C_0 - BK_p R_0 + BK_p C_0\right)
\end{aligned} \tag{B4}$$

The last term in equation (B4) can be expressed in equation (B5):

$$I_0 = C_0 - AC_0 - BK_i \frac{\Delta t}{2} R_0 + BK_i \frac{\Delta t}{2} C_0 - BK_p R_0 + BK_p C_0 \qquad \text{(B5)}$$

Replace equation (B5) into equation (B4), and equation (B6) is obtained:

$$
\begin{aligned}
C_{n+1} = \ & C_n\left(A - BK_p + BK_i \frac{\Delta t}{2}\right) + R_n\left(BK_p - BK_i \frac{\Delta t}{2}\right) \\
& + BK_i \Delta t\left(\sum_{j=0}^{n} R_j - \sum_{j=0}^{n} C_j\right) + I_0
\end{aligned}
\qquad \text{(B6)}
$$

Equation (B6) demonstrates the relationship between the skin temperature $C$ and the thermal setpoint $R$ in the time domain.

# APPENDIX C
## Derivation of Thermal Control Transfer Function

In order to derive the transfer function of the thermal control system, the $z$-transform of discrete equation (22) is taken. In this appendix, equation (22) is written as equation (C1):

$$C_{n+1} = C_n\left(A - BK_p + BK_i\frac{\Delta t}{2}\right) + R_n\left(BK_p - BK_i\frac{\Delta t}{2}\right) +$$
$$BK_i\Delta t\left(\sum_{j=0}^{n} R_j - \sum_{j=0}^{n} C_j\right) + I_0 \tag{C1}$$

The $z$-transforms for the two terms $\sum_{j=0}^{n} R_j$ and $\sum_{j=0}^{n} C_j$ in equation (C1) are complicated; therefore, extra intermediate steps are needed to make it easy to understand. The term $\sum_{j=0}^{n} R_j$ is expanded as follows in equation (C2):

$$\sum_{j=0}^{n} R_j = R_0 + R_1 + \ ...\ + R_n \tag{C2}$$

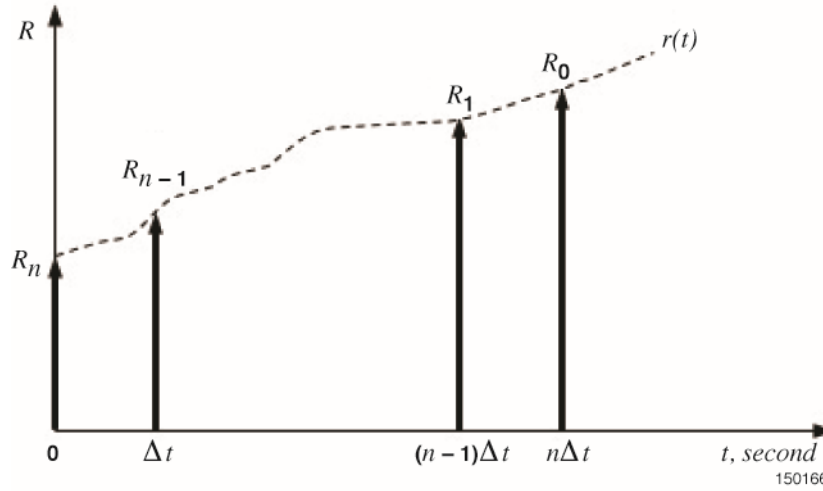From equation (C2), the term $\sum_{j=0}^{n} R_j$ can be represented graphically in figure C1 below.



Figure C1. Graphical representation of $\sum_{j=0}^{n} R_j$ .

Let $u(t)$ be the unit step function occurring at $t = j\Delta t$ as shown in equation (C3):

$$u(t - j\Delta t) = 1 \text{ at } t = j\Delta t \qquad\qquad (j = 1, 2, ..., n) \tag{C3}$$

40

$\sum_{j=0}^{n} R_j$ can be represented as a discrete convolution of $r(t)$ and $u(t)$ as demonstrated in equations (C4) and (C5):

$$\sum_{j=0}^{n} R_j = r(0)u(t - n\Delta t) + r(1)u(t - (n-1)\Delta t) + \; + r(n)u(0) \tag{C4}$$

$$\sum_{j=0}^{n} R_j = \sum_{j=0}^{n} r(j)u(n - j) \tag{C5}$$

Similarly, $\sum_{j=0}^{n} C_j$ can be represented as a discrete convolution of $c(t)$ and $u(t)$ as expressed in equation (C6):

$$\sum_{j=0}^{n} C_j = \sum_{j=0}^{n} c(j)u(n - j) \tag{C6}$$

By using the discrete convolution technique (ref. 2), the $z$-transforms of $\sum_{j=0}^{n} R_j$ and $\sum_{j=0}^{n} C_j$ are as follows in equations (C7) and (C8):

$$z(\sum_{j=0}^{n} R_j) = R(z)\left(\frac{z}{z-1}\right) = \frac{R(z)}{1 - z^{-1}} \tag{C7}$$

$$z(\sum_{j=0}^{n} C_j) = C(z)\left(\frac{z}{z-1}\right) = \frac{C(z)}{1 - z^{-1}} \tag{C8}$$

The z-transform of $C_{n+1}$ can be written as follows in equation (C9):

$$z(C_{n+1}) = z(C(z) - C_0) \tag{C9}$$

Take $z$-transform of equation (C1), and equation (C10) is achieved:

$$z(C(z) - C_0) = C(z)\left( A\text{-}BK_p + BK_i \frac{\Delta t}{2} \right) +$$
$$R(z)\left( BK_p - BK_i \frac{\Delta t}{2} \right) + \tag{C10}$$
$$BK_i \Delta t\left( \frac{R(z)}{1 - z^{-1}} - \frac{C(z)}{1 - z^{-1}} \right) + \frac{I_0}{1 - z^{-1}}$$

Replace z with $\dfrac{1}{z^{-1}}$ into equation (C10), and equation (C11) is obtained:

$$\frac{1}{z^{-1}}\left(C(z)-C_0\right)=C(z)\left(A-BK_p+BK_i\frac{\Delta t}{2}\right)+$$
$$R(z)\left(BK_p-BK_i\frac{\Delta t}{2}\right)+ \tag{C11}$$
$$BK_i\Delta t\left(\frac{R(z)}{1-z^{-1}}-\frac{C(z)}{1-z^{-1}}\right)+\frac{I_0}{1-z^{-1}}$$

Multiply the left-hand side and the right-hand side terms with $z^{-1}$ or $\left(1-z^{-1}\right)$ or $z^{-1}\left(1-z^{-1}\right)$ so that both sides have the common denominator of $z^{-1}\left(1-z^{-1}\right)$ to obtain equation (C12):

$$\left(1-z^{-1}\right)\left(C(z)-C_0\right)=z^{-1}\left(1-z^{-1}\right)C(z)\left(A-BK_p+BK_i\frac{\Delta t}{2}\right)+$$
$$z^{-1}\left(1-z^{-1}\right)R(z)\left(BK_p-BK_i\frac{\Delta t}{2}\right)+ \tag{C12}$$
$$z^{-1}BK_i\Delta t\left(R(z)-C(z)\right)+z^{-1}I_0$$

Expand the above equation and combine the alike terms, and equations (C13)–(C15) are obtained:

$$C(z)\left[1-z^{-1}-z^{-1}\left(1-z^{-1}\right)\left(A-BK_p+BK_i\frac{\Delta t}{2}\right)+z^{-1}BK_i\Delta t\right]=$$
$$R(z)\left[z^{-1}\left(1-z^{-1}\right)\left(BK_p-BK_i\frac{\Delta t}{2}\right)+z^{-1}BK_i\Delta t\right]+ \tag{C13}$$
$$z^{-1}\left[I_0-C_0\right]+C_0$$

$$C(z)\left[1-z^{-1}-\left(z^{-1}-z^{-2}\right)\left(A-BK_p+BK_i\frac{\Delta t}{2}\right)+z^{-1}BK_i\Delta t\right]=$$
$$R(z)\left[\left(z^{-1}-z^{-2}\right)\left(BK_p-BK_i\frac{\Delta t}{2}\right)+z^{-1}BK_i\Delta t\right]+ \tag{C14}$$
$$z^{-1}\left(I_0-C_0\right)+C_0$$

$$C(z)\left[1-z^{-1}\left(1+A-BK_p-BK_i\frac{\Delta t}{2}\right)+z^{-2}\left(A-BK_p+BK_i\frac{\Delta t}{2}\right)\right]=$$

$$R(z)\left[z^{-1}\left(BK_p+BK_i\frac{\Delta t}{2}\right)-z^{-2}\left(BK_p-BK_i\frac{\Delta t}{2}\right)\right]+ \tag{C15}$$

$$z^{-1}(I_0-C_0)+C_0$$

Equation (C15) is the *z*-transform of the skin temperature *C(z)* and the thermal setpoint *R(z)*. Equation (C15) will be used to derive the thermal control transfer function.

# APPENDIX D
## Determination of Thermal Control System Stability

To determine the TCS stability, the relationships between the integral sensitivity factor α, the proportional sensitivity factor β, the poles $z_1$, and $z_2$, in equation (D1) and equation (D2) must be solved where $\alpha, \beta > 0$, and $0 < z_1,\ z_2 < 1$, therefore:

$$0 < z_1,z_2 = \frac{\left(2 - \beta - \frac{\alpha\beta}{2}\right) \pm \sqrt{\left(2 - \beta - \frac{\alpha\beta}{2}\right)^2 - 4\left(1 - \beta + \frac{\alpha\beta}{2}\right)}}{2} < 1 \tag{D1}$$

$$\left(2 - \beta - \frac{\alpha\beta}{2}\right)^2 - 4\left(1 - \beta + \frac{\alpha\beta}{2}\right) \geq 0 \tag{D2}$$

### Stability Region 1

Multiply equation (D1) by 2 to obtain equation (D3):

$$0 < \left(2 - \beta - \frac{\alpha\beta}{2}\right) \pm \sqrt{\left(2 - \beta - \frac{\alpha\beta}{2}\right)^2 - 4\left(1 - \beta + \frac{\alpha\beta}{2}\right)} < 2 \tag{D3}$$

Equation (D3) has two-side conditions, so consider the left-hand side in equation (D4):

$$0 < \left(2 - \beta - \frac{\alpha\beta}{2}\right) \pm \sqrt{\left(2 - \beta - \frac{\alpha\beta}{2}\right)^2 - 4\left(1 - \beta + \frac{\alpha\beta}{2}\right)} \tag{D4}$$

Move the square root term in equation (D4) to one side to achieve equation (D5):

$$\mp \sqrt{\left(2 - \beta - \frac{\alpha\beta}{2}\right)^2 - 4\left(1 - \beta + \frac{\alpha\beta}{2}\right)} < 2 - \beta - \frac{\alpha\beta}{2} \tag{D5}$$

Square both sides as shown in equation (D6):

$$\left(2 - \beta - \frac{\alpha\beta}{2}\right)^2 - 4\left(1 - \beta + \frac{\alpha\beta}{2}\right) < \left(2 - \beta - \frac{\alpha\beta}{2}\right)^2 \tag{D6}$$

Remove the $\left(2 - \beta - \frac{\alpha\beta}{2}\right)^2$ term from both sides in equation (D6), and equations (D7) and (D8) are obtained:

$$4\left(1 - \beta + \frac{\alpha\beta}{2}\right) > 0 \tag{D7}$$

$$1 - \beta + \frac{\alpha\beta}{2} > 0 \tag{D8}$$

Move all $\beta$ terms in equation (D8) to the left hand side as shown in equations (D9) and (D10):

$$\beta\left(1 - \frac{\alpha}{2}\right) < 1 \tag{D9}$$

$$0 < \beta < \frac{2}{2 - \alpha} \tag{D10}$$

To satisfy the conditions $0 < \beta$ in equation (D10), the term $2 - \alpha$ in the denominator must be positive as expressed in equation (D11):

$$0 < \alpha < 2 \tag{D11}$$

The boundary conditions of α in equation (D11) will be applied to all stability regions. Equations (D10) and (D11) determine Stability Region 1.

## Stability Region 2

Consider equation (D2):

$$\left(2 - \beta - \frac{\alpha\beta}{2}\right)^2 - 4\left(1 - \beta + \frac{\alpha\beta}{2}\right) \geq 0 \tag{D2}$$

From equation (D8), $1 - \beta + \frac{\alpha\beta}{2} > 0$; therefore, the following condition shown in equations (D12) will always be true:

$$abs\sqrt{\left(2 - \beta - \frac{\alpha\beta}{2}\right)^2 - 4\left(1 - \beta + \frac{\alpha\beta}{2}\right)} < abs\left(2 - \beta - \frac{\alpha\beta}{2}\right) \tag{D12}$$

If $2 - \beta - \frac{\alpha\beta}{2} < 0$, then equation (D12) can be expressed in equation (D13):

$$-abs\sqrt{\left(2 - \beta - \frac{\alpha\beta}{2}\right)^2 - 4\left(1 - \beta + \frac{\alpha\beta}{2}\right)} > \left(2 - \beta - \frac{\alpha\beta}{2}\right) \tag{D13}$$

From the condition of equation (D13), both sides are negative and the left-hand side is less negative than the right-hand side. Therefore, equation (D1) will have both poles $z_1, z_2 < 0$. Based on the selected stability condition that both poles must be greater than zero, the condition in equation (D13) is not acceptable.

If $2 - \beta - \frac{\alpha\beta}{2} > 0$, then equation (D12) can be expressed in equation (D14):

$$abs\sqrt{\left(2-\beta-\frac{\alpha\beta}{2}\right)^2-4\left(1-\beta+\frac{\alpha\beta}{2}\right)}<\left(2-\beta-\frac{\alpha\beta}{2}\right) \tag{D14}$$

From the condition of equation (D14), both sides are positive and the left-hand side is less positive than the right-hand side. Therefore, equation (D1) will have both poles $z_1$, $z_2 > 0$ which satisfy the left-hand side of the selected stability condition as shown in equation (D15):

$$2-\beta-\frac{\alpha\beta}{2}>0 \tag{D15}$$

Move all $\beta$ terms in equation (D15) to one side, equations (D16) and (D17) are derived:

$$2>\beta\left(1+\frac{\alpha}{2}\right) \tag{D16}$$

$$0<\beta<\frac{4}{2+\alpha} \tag{D17}$$

The boundary conditions of $0<\alpha<2$ in equation (D11) produces the boundary conditions of $\beta$ as shown in equation (D18):

$$0<\beta<2 \tag{D18}$$

Check if the condition $2-\beta-\frac{\alpha\beta}{2}>0$ in equation (D15) satisfies the right-hand side of equation (D1):

$$\left(2-\beta-\frac{\alpha\beta}{2}\right)\pm\sqrt{\left(2-\beta-\frac{\alpha\beta}{2}\right)^2-4\left(1-\beta+\frac{\alpha\beta}{2}\right)}<2 \tag{D1}$$

Move the $2-\beta-\frac{\alpha\beta}{2}$ term in equation (D1) to the right-hand as shown in equation (D19):

$$\pm\sqrt{\left(2-\beta-\frac{\alpha\beta}{2}\right)^2-4\left(1-\beta+\frac{\alpha\beta}{2}\right)}<2-\left(2-\beta-\frac{\alpha\beta}{2}\right) \tag{D19}$$

Square both sides of equation (D19), and equation (D20) is derived:

$$\left(2-\beta-\frac{\alpha\beta}{2}\right)^2-4\left(1-\beta+\frac{\alpha\beta}{2}\right)<4-4\left(2-\beta-\frac{\alpha\beta}{2}\right)+\left(2-\beta-\frac{\alpha\beta}{2}\right)^2 \tag{D20}$$

Eliminate $\left(2-\beta-\frac{\alpha\beta}{2}\right)^2$ term and divide by 4, and equation (D21) is obtained:

46

$$-\left(1-\beta+\frac{\alpha\beta}{2}\right)<1-\left(2-\beta-\frac{\alpha\beta}{2}\right) \tag{D21}$$

From equation (D15), $2-\beta-\frac{\alpha\beta}{2}>0$; therefore, the following condition in equations (D22) and (D23) will always be true:

$$1-\left(2-\beta-\frac{\alpha\beta}{2}\right)<1 \tag{D22}$$

$$\left(1-\beta-\frac{\alpha\beta}{2}\right)>-1 \tag{D23}$$

The conditions in equations (D22) and (D23) satisfy the right-hand side condition of equation (D1). Therefore, the condition $2-\beta-\frac{\alpha\beta}{2}>0$ satisfies both left-hand and right-hand sides of equation (D1). Equations (D17) and (D18) determine Stability Region 2.

**Stability Region 3**

Expand equation (D2) as shown in equation (D24):

$$4+\beta^2+\frac{\alpha^2\beta^2}{4}-4\beta-2\alpha\beta+\alpha\beta^2-4+4\beta-2\alpha\beta\geq0 \tag{D24}$$

Eliminate terms 4 and 4$\beta$ and rearrange the similar terms in equation (D24), and equation (D25) is obtained:

$$\beta\left(\frac{\alpha^2\beta}{4}+\alpha\beta+\beta-4\alpha\right)\geq0 \tag{D25}$$

Since $\beta>0$, the term inside the bracket must be $\geq0$ as shown in equation (D26):

$$\frac{\alpha^2\beta}{4}+\alpha\beta+\beta-4\alpha\geq0 \tag{D26}$$

Move all $\beta$ terms in equation (D26) to one side, equation (D27) is derived:

$$\frac{\beta}{4}\left(\alpha^2+4\alpha+4\right)\geq4\alpha \tag{D27}$$

Rewrite the above equation in a more compact form as shown in equation (D28):

$$\frac{\beta}{4}(\alpha+2)^2 \geq 4\alpha \qquad \text{(D28)}$$

Move all α terms in equation (D28) to the right-hand side, and equation (D29) is achieved:

$$\beta \geq \frac{16\alpha}{(\alpha+2)^2} \qquad \text{(D29)}$$

Equation (D29) determines Stability Region 3.

The graphs for the stability regions in figures D1, D2, and D3 are limited to $0 < \alpha < 2$ and $0 < \beta < 2$ base on equations (D11) and (D18).
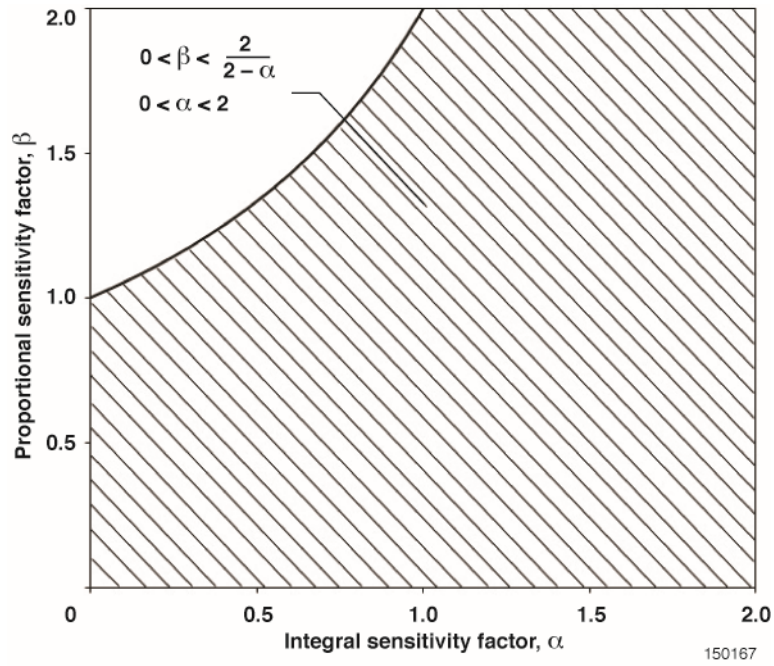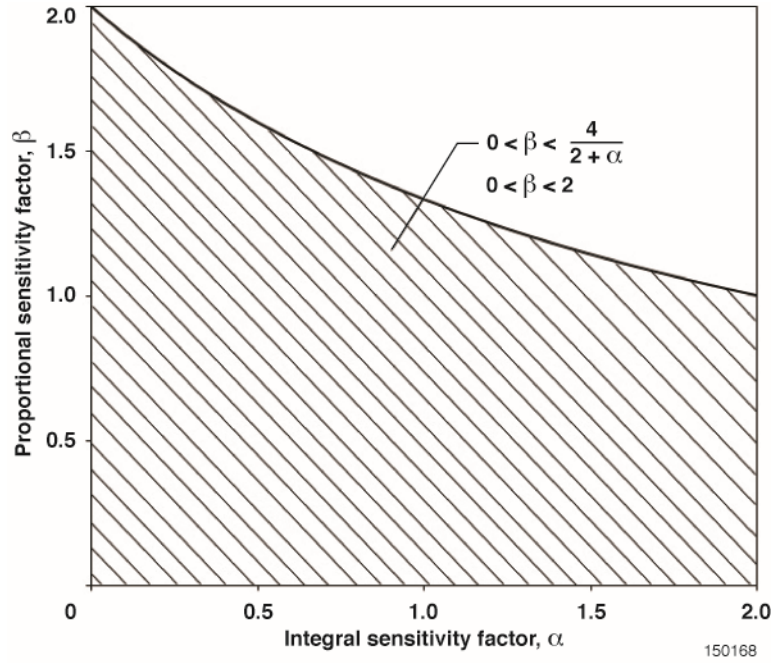


Figure D1. Stability Region 1.

$$0 < \beta < \frac{4}{2 + \alpha}$$

$$0 < \beta < 2$$

Figure D2. Stability Region 2.
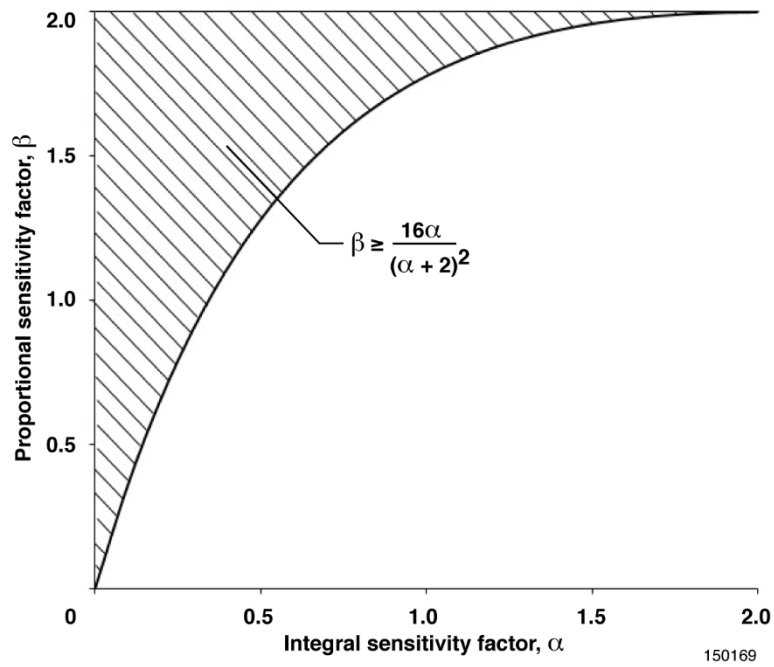


$$\beta \geq \frac{16\alpha}{(\alpha + 2)^2}$$

Figure D3. Stability Region 3.

By superimposing all stability regions, one overlapped stability region is defined and shown in figure 7. Since many assumptions has been made during the development process, only conservative values for $\alpha$ and $\beta$ should be chosen.

# APPENDIX E
## A Thermal Profile

A thermal profile is very important in thermal tests. It consists of at least one segment that has a straight line relationship between temperature and time. In each segment, there are start time, end time, start temperature, and end temperature. The segment slope in °F/s is computed as follows:

$$slope = \frac{end\ temperature - start\ temperature}{end\ time - start\ time}$$

and the profile temperature is calculated with $t$ is THRM PET in seconds:

*profile temperature = slope \* (t – start temperature) + start temperature*

Table E1 below describes how a typical thermal profile is created for each zone.

Table E1. Thermal profile used in implementing GH closed-loop thermal control.

| Segment number | Start time, second | End time, second | Start temperature, °F | End temperature, °F |
|---|---|---|---|---|
| | | | Ambient | 80 |
| 1 | 0 | 100 | 80 | 230 |
| 2 | 100 | 200 | 230 | 530 |
| 3 | 200 | 300 | 530 | 980 |
| 4 | 300 | 400 | 980 | 1280 |
| 5 | 400 | 500 | 1280 | 1480 |
| 6 | 500 | 800 | 1480 | 1480 |
| 7 | 800 | 1000 | 1480 | 1380 |
| 8 | 1000 | 1200 | 1380 | 1180 |

# REFERENCES

1.  Kuo, Benjamin C., *Automatic Control Systems, Fourth Edition*, Prentice-Hall, Inc., Englewood Cliffs, N.J. 1982, pages 1-16 and 51-61.

2.  Phillips, Charles L., and Nagle, H. Troy Jr., *Digital Control System Analysis and Design*, Prentice-Hall, Inc., Englewood Cliffs, N.J. 1984, pages 1-3, 19-22, 30-34, and 191.

3.  DACS III Software Engineering Team, Computer Sciences Corporation, *Software Requirements Specification for the Thermostructural Laboratory DACS III*, Edwards, California, July 30, 1993.

4.  DACS III Software Engineering Team, Woodside Summit Group, Inc., *DACS III System Software/Hardware Training Reference*, June 26, 1998.

5.  *SCR Power Theory Training Manual*, Chromalox Inc., LaVergne, Tennessee, 1997-2001, pages 3-13.